Synthesis, Evaluation, and Comparative Molecular Field Analysis of 1-Phenyl-3-amino-1,2,3,4-tetrahydronaphthalenes as Ligands for Histamine H_1 Receptors

Ehren C. Bucholtz, Randal L. Brown, Alexander Tropsha, Raymond G. Booth, and Steven D. Wyrick*

Division of Medicinal Chemistry and Natural Products, School of Pharmacy, CB# 7360, University of North Carolina, Chapel Hill, North Carolina 27599-7360

Received July 24, 1998

A series of 1-phenyl-3-amino-1,2,3,4-tetrahydronaphthalenes (1-phenyl-3-aminotetralins, PATs) previously was found to modulate tyrosine hydroxylase activity and dopamine synthesis in rodent forebrain through interaction with a binding site labeled by [^{3}H]-(−)-(1*R*,3*S*)-*trans*-H_2-PAT. Recently, we have discovered that PATs also bind with high affinity to the [^{3}H]-mepyramine-labeled H_1 receptor in rat and guinea pig brain. Here, we report the synthesis and biological evaluation of additional PAT analogues in order to identify differences in binding at these two sites. Further molecular modifications involve the pendant phenyl ring as well as quaternary amine compounds. Comparison of about 38 PAT analogues, 10 structurally diverse H_1 ligands, and several other CNS-active compounds revealed no significant differences in affinity at [^{3}H]-(−)-*trans*-H_2-PAT sites versus [^{3}H]mepyramine-labeled H_1 receptors. These results, together with previous autoradiographic brain receptor-mapping studies that indicate similar distribution of [^{3}H]-(−)-*trans*-H_2-PAT sites and [^{3}H]mepyramine-labeled H_1 receptors, suggest that both radioligands label the same histamine H_1 receptors in rodent brain. We also report a revision of our previous comparative molecular field analysis (CoMFA) study of the PAT ligands that yields a highly predictive model for 66 compounds with a cross-validated R^2 (q^2) value of 0.67. This model will be useful for the prediction of high-affinity ligands at radiolabeled H_1 receptors in mammalian brain.

Introduction

The phenylaminotetralins (PATs) (±)-*trans*-1-phenyl-3-(dimethylamino)-1,2,3,4-tetrahydronaphthalene (*trans*-H_2-PAT, **1**; Chart 1) and (±)-*trans*-6-chloro-7-hydroxy-1-phenyl-3-(dimethylamino)-1,2,3,4-tetrahydronaphthalene (Cl, OH-PAT, **2**; Chart 1) stimulate tyrosine hydroxylase activity and dopamine (DA) synthesis in rodent brain in vitro.[1] It is hypothesized that this effect is mediated through interaction with a CNS binding site that is labeled by [^{3}H]-(±)-*trans*-Cl,OH-PAT.[2] This site was designated originally as the PAT-σ_3 receptor, because although it had low affinity for σ_1/σ_2 ligands, it incorporated a σ-like pharmacophore, it had a σ-like rodent brain distribution, and its functional effects on dopamine synthesis were blocked by the σ antagonist BMY-14802. While (±)-Cl,OH-PAT-induced stimulation of tyrosine hydroxylase is accompanied by nonspecific effects on dopamine release, (±)-*trans*-H_2-PAT effects at 0.1−10 μM, are confined to stimulation of dopamine synthesis. Consequently, the enantiomers of (±)-*trans*-H_2-PAT were resolved, and stimulation of tyrosine hydroxylase and DA synthesis activity at 0.1 μM was found to reside in the (−)-*trans*-(1*R*,3*S*) enantiomer.[2] This enantiomer also exhibited 40-fold greater affinity for the PAT-σ_3 receptor when compared to the (+)-(1*S*,3*R*) enantiomer. Moreover, preliminary studies indicated that at 0.1 μM, (±)-*cis*-H_2-PAT did not stimulate tyrosine hydroxylase and had about 5-fold less affinity for [^{3}H]-(±)-*trans*-Cl,OH-PAT sites.[2] These data suggested a dependence between chirality, receptor interaction, and functional effects. Consequently, the stereoselective radioligand, [^{3}H]-(−)-(1*R*,3*S*)-*trans*-H_2-PAT, was synthesized and used to label PAT-σ_3 sites in all subsequent radioreceptor studies.[3]

Chart 1. *trans*-H_2-PAT (left) and *trans*-Cl,OH-PAT (right)

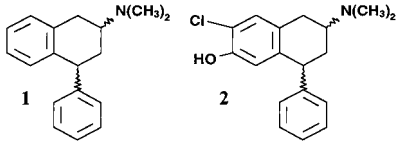

Recently, radioreceptor assays indicated that (−)-*trans*-H_2-PAT also has high affinity ($K_{0.5}$ = 1.6 nM) for histamine H_1 receptors and that the pharmacological profile of [^{3}H]-(−)-*trans*-H_2-PAT sites is similar to that of H_1 receptors.[4−6] We discovered, for example, that the distribution and rank order of ligand binding at [^{3}H]-(−)-*trans*-H_2-PAT sites is more comparable but not identical to [^{3}H]mepyramine-labeled H_1 sites versus [^{3}H]ditolylguanidine (DTG)-labeled σ_1/σ_2 sites in guinea pig brain.[7] These observations, taken together with recent molecular cloning evidence[8,9] suggesting that σ sites are not closely related to other known mammalian neurotransmitter receptors, led us to hypothesize that [^{3}H]-(−)-*trans*-H_2-PAT sites may actually represent brain histamine H_1-type receptors.

(−)-*trans*-H_2-PAT incorporates the pharmacophore present in the four prototypical structural classes of histamine H_1 antagonists: the ethylenediamines, the

* To whom correspondence should be addressed.

10.1021/jm980428x CCC: $18.00
Published on Web 07/16/1999

Table 1. Binding Affinity of PAT Analogues Used in CoMFA/q^2-GRS Studies of the [^{3}H]-(−)-*trans*-H_2-PAT Binding Site

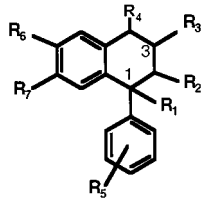

									$K_{0.5}$ (nM)	
compd	config[a]	R_1	R_2	R_3	R_4	R_5	R_6	R_7	PAT[b]	H_1[c]
1a	(−)-*trans*	H	H	$N(CH_3)_2$	CH_2	H	H	H	0.33 ± 0.09[d]	1.07 ± 0.24[d]
1b	(+)-*trans*	H	H	$N(CH_3)_2$	CH_2	H	H	H	13.6 ± 2.1[d]	19.1± 1.6[d]
1c	(−)-*cis*	H	H	$N(CH_3)_2$	CH_2	H	H	H	2.9 ± 0.4[d]	2.45 ± 0.13[d]
1d	(+)-*cis*	H	H	$N(CH_3)_2$	CH_2	H	H	H	70.4 ± 8.1[d]	111 ± 3.5[d]
2	(±)-*trans*	H	H	$N(CH_3)_2$	CH_2	H	Cl	OH	0.63 ± 0.05	1.47 ± 0.20
3	(±)-*trans*	H	H	$N(CH_3)_3$	CH_2	H	H	H	35 ± 2.5	120 ± 15
4	(±)-*trans*	H	H	$NH(CH_3)$	CH_2	H	H	H	112 ±_31	64 ± 10
5	(±)-*trans*	H	H	$N(C_2H_5)_2$	CH_2	H	H	H	5.7 ± 0.4	13.3 ± 1.37
6	(±)-*trans*	H	H	$NCH_3(C_3H_5)$	CH_2	H	H	H	3.4 ± 0.3[f]	ND
7	(±)-*trans*	H	H	$N(C_3H_5)_2$	CH_2	H	H	H	10.2 ± 1.7[f]	ND
8	(±)-*cis*	H	$N(CH_3)_2$	H	CH_2	H	H	H	1200 ± 100	>2000
9	(±)-*trans*	H	$N(CH_3)_2$	H	CH_2	H	H	H	940 ± 53	ND
10	(±)-*cis*	H	H	$N(CH_3)_2$	C_2H_4	H	H	H	109 ± 13	217 ± 49
11	(±)-*trans*	H	H	$N(CH_3)_2$	C_2H_4	H	H	H	20.9 ± 2.4[e]	ND
12	(±)-*trans*	H	H	$N(CH_3)_2$	CH_2	H	OH	OH	60 ± 5.8	69 ± 4.2
13	(±)-*cis*	H	H	$N(CH_3)_2$	CH_2	H	OH	OH	9.6 ± 1.7	11.8 ± 2.4
14	(±)-*trans*	CH_3	H	$N(CH_3)_2$	CH_2	H	H	H	18.3 ± 1.9	40 ± 5.0
15	(±)-*cis*	CH_3	H	$N(CH_3)_2$	CH_2	H	H	H	1.90 ± 0.50	4.4 ± 1.1
16	(±)-*trans*	H	H	$NCH_3((CH_2)_2C_6H_5)$	CH_2	H	H	H	140 ± 24[e]	ND
17	(±)-*trans*	H	H	$NCH_3((CH_2)_3C_6H_5)$	CH_2	H	H	H	333 ± 33[e]	ND
18	(±)-*trans*	H	H	$NCH_3((CH_2)_4C_6H_5)$	CH_2	H	H	H	212 ± 39[e]	ND
20	(±)-*trans*	H	H	$N(CH_3)_2$	CH_2	*o*-Cl	H	H	53 ± 11.2	42.7 ± 4.7
21	(±)-*trans*	H	H	$N(CH_3)_2$	CH_2	*o*-CH_3	H	H	10.2 ± 1.7	12.7 ± 0.6
22	(±)-*trans*	H	H	$N(CH_3)_2$	CH_2	*p*-Cl	H	H	9.0 ± 2.8	4.4 ± 1.6
23	(±)-*trans*	H	H	$N(CH_3)_2$	CH_2	*p*-CH_3	H	H	2.47 ± 0.23	5.0 ± 0.4
24	(±)-*trans*	H	H	$N(CH_3)_2$	CH_2	*p*-F	H	H	1.53 ± 0.10	2.3 ± 0.1
25	(±)-*cis*	H	H	$N(CH_3)_3$	CH_2	H	H	H	117 ± 2.8	107 ± 4.1
28	(±)-*cis*	H	H	$N(CH_3)_2$	CH_2	H	Cl	OH	0.54 ± 0.1[f]	ND
29	(±)-*cis*	H	H	NH_2	CH_2	H	OH	OH	>5000[f]	ND
30	(±)-*trans*	H	H	$NH(CH_3)$	CH_2	H	Cl	OH	8.1 ± 0.8[f]	ND
31	(±)-*trans*	H	H	$NH(C_3H_5)$	CH_2	H	H	H	45 ± 11[f]	ND
32	(±)-*trans*	H	H	$NH(CH_2)_3C_6H_5$	CH_2	H	H	H	2500 ± 400[e]	ND
33	(±)-*trans*	H	H	$NH(CH_2)_4C_6H_5$	CH_2	H	H	H	1500 ± 200[e]	ND
34	(±)-*trans*	H	H	NH_2	CH_2	H	OH	OH	>5000[f]	ND
35	(±)-*trans*	H	H	NH_2	CH_2	H	H	H	1270 ± 92	ND

[a] Configuration (config) *cis* or *trans* denotes the relationship of substituents at positions 1 and 3. [b] Versus [^{3}H]-(−)-*trans*-H_2-PAT. [c] Versus [^{3}H]mepyramine. [d] Reference 12. [e] Reference 10. [f] Reference 2. ND, not determined.

aminoalkyl ethers, the semirigid 1,1-diaryl-3-(alkylamino)propenes, and the 1,1-diaryl-(3-alkylamino)propanes.[10] Functionally, H_1 antagonists have been characterized by their ability to block histamine-induced contraction of guinea pig ileum. Structure−activity relationships (SAR) for H_1 antagonists have been reviewed elsewhere.[10−14]

SARs for the [^{3}H]-(−)-*trans*-H_2-PAT binding site have revealed little steric tolerance for amine substituents; a dimethyl substitution is optimal for high affinity. *N*,*N*,*N*-Trimethyl (quaternary, **3**), *N*-methyl (**4**), *N*,*N*-diethyl (**5**), *N*-allyl-*N*-methyl (**6**), and *N*,*N*-diallyl (**7**) PATs all have reduced affinity at the site compared to (±)-*trans*-H_2-PAT. The effect of altering the position of the amino group was investigated by designing PAT analogues with the amine in position 2 of the tetrahydronaphthalene and by making ring-expanded benzocycloheptyl-PAT analogues.[15] The *cis*- and *trans*-1-phenyl-2-aminotetralins (**8** and **9**; Table 1) exhibit an approximately 1000-fold decrease in affinity, indicating a proper spatial orientation of the 3-amine relative to the aromatic substituents is important for binding. The *cis*- and *trans*-benzocycloheptyl-PATs (**10** and **11**, respectively) which expand the tetralin ring also have moderately reduced affinity compared to (±)-*trans*-H_2-PAT, perhaps due to a less drastic alteration of the 3-amino position as compared to the 2-amino analogues (**8** and **9**) of *trans*-H_2-PAT. Aromatic substitutions, such as 6-chloro-7-hydroxy (**2**), retain high binding affinity. However, catechol analogues (**12** and **13**) were found to exhibit reduced affinity at this site compared to **2**. The *trans*- and *cis*-1-methyl-1-phenyl-3-(dimethylamino)tetralins (**14** and **15**) also showed reduced affinity compared to (±)-*trans*-H_2-PAT by approximately 1 order of magnitude.

Molecular modeling studies were performed on these PATs as well as various non-PAT ligands with a wide range of affinities for the [^{3}H]-(−)-*trans*-H_2-PAT binding site.[16] A pharmacophore mapping program (distance comparison, DISCO)[17] was utilized to identify structural features that are common to ligands that bind to the PAT binding site and to develop a ligand binding model. The resulting alignment was utilized in a comparative molecular field analysis (CoMFA) study to correlate the

steric and electrostatic fields with affinity for the PAT site. A cross-validated R^2 (q^2) of 0.61 was obtained indicating a model with a high degree of internal predictability. Visualization of the volumes that contribute to the affinities of the active versus less active compounds indicated that an auxiliary binding pocket may exist that can accommodate large phenylalkyl nitrogen substituents. To test this model, we synthesized *trans*-H_2-PATs that included 2-phenylethyl (**16**), 3-phenylpropyl (**17**), and 4-phenylbutyl (**18**) nitrogen substituents. In competition binding assays, not only did these PAT analogues have markedly reduced affinity for the PAT binding site ($K_{0.5}$ = 150, 300, and 280 nM, respectively), but they also exhibited increased affinity for dopamine and σ receptors.[15] This erroneous prediction of high affinity for phenylalkyl-substituted PATs was most likely due to the fact that these new ligands extended beyond the probed receptor space. These data suggest that further refinement of the reported binding model is required.

Since reporting our previous binding model, we also have learned more about how stereochemistry affects binding at this site. (−)-*trans*-H_2-PAT (**1a**; Table 1) and (−)-*cis*-H_2-PAT (**1c**) have higher affinity, as compared to their corresponding (+) isomers (**1b** and **1d**, respectively). The rank order of binding of H_2-PAT isomers is (1*R*,3*S*) (**1a**) > (1*S*,3*S*) (**1c**) > (1*S*,3*R*) (**1b**) > (1*R*,3*R*) (**1d**), suggesting that chirality (*S* configuration) at the C3 amine position (shared by both (−)-*cis*- and (−)-*trans*-H_2-PAT) is an important structural determinate for high affinity of PAT-type molecules at PAT binding sites. [18]

We have undertaken further SAR studies here to identify differences between the classical [^{3}H]mepyramine-labeled H_1 sites and [^{3}H]-(−)-*trans*-H_2-PAT-labeled sites to test our hypothesis that [^{3}H]-(−)-*trans*-H_2-PAT may represent histamine H_1-type receptors. Using (±)-*trans*-H_2-PAT as a probe, we have compared the SAR of the classical [^{3}H]mepyramine-labeled H_1 sites and [^{3}H]-(−)-*trans*-H_2-PAT-labeled sites. Structural modifications to (±)-*trans*-H_2-PAT (analogues **19**−**24**; Tables 1 and 2) address steric and electrostatic requirements of the pendant phenyl ring. The 2-aminotetralin **19** (Table 2, Chart 2) tests if the pendent phenyl is a requirement for binding. The substituted pendent phenyl ring compounds **20**−**24** (Table 1) address the effects on binding of steric or electrostatic variation on the pendent phenyl ring and provide insight as to determine how nonrigid compounds with aromatic substituents bind to the two sites. The *cis*-trimethylammonium quaternary analogue **2** (Table 1**)** of **1** tests further if quaternization of the amine reduces affinity for these two sites. The 3-aminofluoranthenes **26** and **27** (Table 2, Chart 2) investigate the importance of the coplanarity of the diaryl ring system and the relative position of the amine group. We also have completed competition binding assays to assess binding of 6,7-substituted compounds (**2**, **12**, and **13**; Table 1) as well as numerous other PAT ligands to the [^{3}H]mepyramine-labeled H_1 sites which previously have been analyzed at the [^{3}H]-(−)-*trans*-H_2-PAT-labeled sites.[2,15,18]

The synthesis and biological evaluation of these nine new PATs (**19**−**27**) reported in this paper have been used together with 57 (Tables 1 and 2) other PAT analogues (**1**−**18**, **28**−**35**) synthesized and tested earlier[2,15,18] and non-PAT compounds (**36**−**63**, Chart 2) to develop a revised and extended CoMFA model for ligand binding at the [^{3}H]-(−)-*trans*-H_2-PAT-labeled sites. The new model is characterized by a high q^2 value of 0.68 which slightly exceeds the q^2 value (0.61) obtained for a previous CoMFA model.[16] This new CoMFA model for ligand binding to [^{3}H]-(−)-*trans*-H_2-PAT-labeled sites of PAT ligands provides new insights into the specificity of PAT binding and facilitates the design of novel PAT ligands. These SAR studies will help to increase our understanding of brain histamine H_1-type receptors and to investigate the role histamine plays as a brain neurotransmitter.

Table 2. Binding Affinity of Non-PATs Used in CoMFA/q^2-GRS Studies of the [^{3}H]-(−)-*trans*-H_2-PAT Binding Site

	$K_{0.5}$ (nM)	
compd	PAT[a]	H_1[b]
19, 2-(dimethylamino)tetralin	165 ± 24	75 ± 4.7
26, 3-aminofluoranthene	ca. 4800	ca. 4000
27, 3-(dimethylamino)fluoranthene	ca. 4800	ca. 4000
36, diphenhydramine	4.1 ± 0.41	6.1 ± 1.7
37, (+)-butaclamol	147 ± 13	405 ± 76
38, (*R*)-chlorpheniramine	20.9 ± 2.9	61.6 ± 6.4
39, (*S*)-chlorpheniramine	0.31 ± 0.03	1.16 ± 0.37
40, triprolidine	0.12 ± 0.03	0.46 ± 0.05
41, atropine	1236 ± 177	580 ± 52
42, (−)-NANM	>5000	ca. 2000
43, doxepin	0.06 ± 0.01	0.16 ± 0.04
44, *cis*-flupenthixol	0.86 ± 0.17[c]	ND
45, *trans*-flupenthixol	5.73 ± 0.85[c]	ND
46, mazindol	ca. 600	ND
47, SCH-23390	101 ± 14	ND
48, methysergide	ca. 3000	ND
49, SKF-38393	ca. 2500	ND
50, amytriptyline	0.50 ± 0.03	ND
51, desipramine	45.4 ± 1.8	ND
52, 7-OH-DPAT	ca. 1500	ND
53, haloperidol	215 ± 20	ND
54, loperamine	ca. 2000	ND
55, mianserin	0.30 ± 0.07	ND
56, rimcazole	>5000	ND
57, spiperone	272 ± 48	ND
58, ketanserin	1.79 ± 0.05	ND
59, promethazine	0.24 ± 0.06	ND
60, mepyramine	0.58 ± 0.28	0.53 ± 0.12
61, GBR-12909	9.33 ± 1.66	ND
62, nortryptyline	15.1 ± 5.6	ND
63, (±) BMY-14802	180 ± 14	548 ± 187

[a] Versus [^{3}H]-(−)-*trans*-H_2-PAT. [b] Versus [^{3}H]mepyramine. [c] Reference 1.

Chemical Synthesis

Synthesis of 2-aminotetralin **19** (Scheme 1) was initiated by reduction of β-tetralone (**64**) which yielded the 2-tetralol (**65**). This was converted to the tosylate and subsequently treated with sodium azide to afford the 2-azido-1,2,3,4-tetrahydronaphthalene (**66**) by the procedure of Laus.[19] The azide was reduced to the primary amine **67** and converted to the 2-(dimethylamino)-1,2,3,4-tetrahydronaphthalene (**19**) by the method of Eschweiler.[20] The synthetic path used for synthesis of *ortho*- and *para*-substituted PATs was identical to that previously reported for Cl,OH-PAT and H_2-PAT.[2,4]

Computational Methods

SYBYL molecular modeling software[21] was used for structure generation and CoMFA.[22] For this work, we have selected 66 chemically diverse ligands that bind to the histamine H_1 receptor (Tables 2 and 3) whose

Chart 2. Non-PATs Used in Molecular Modeling Studies

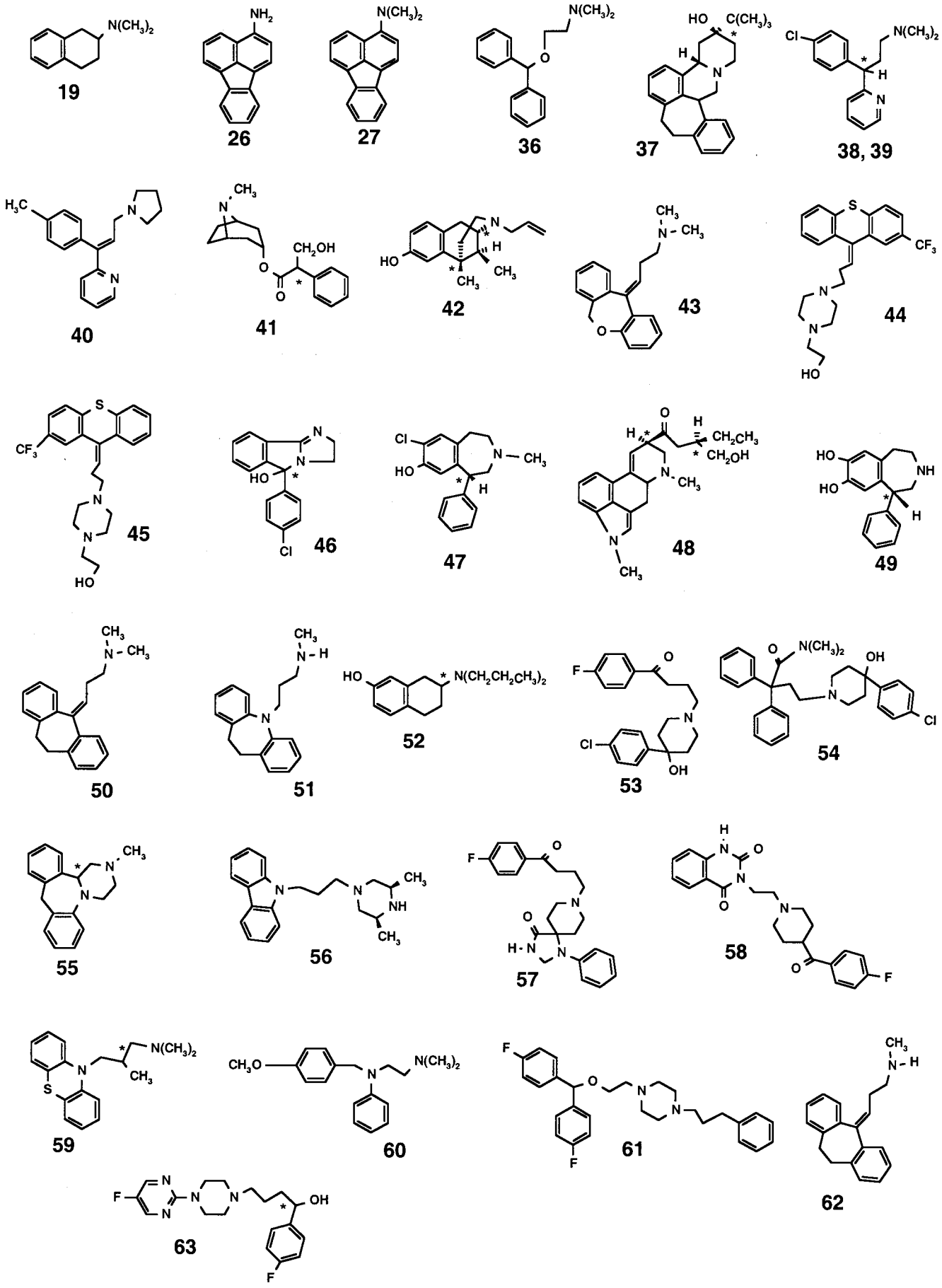

Table 3. q^2 and SDEP (numbers in parentheses) Values Obtained after Performing CoMFA/q^2-GRS with Different q^2 Cutoff Values[a]

			no. of components					
dataset	q^2 cutoff	lattice points	1	2	3	4	5	6
training	none[b]	1210	0.050 (1.339)	0.377 (1.095)	**0.460 (1.031)**	0.425 (1.076)	0.398 (1.113)	0.404 (0.120)
training	0.1	700	0.136 (1.238)	0.441 (1.006)	0.451 (1.008)	0.472 (0.999)	0.503 (0.978)	**0.513 (0.982)**
training	0.15	600	0.122 (1.248)	**0.344 (1.090)**	0.274 (1.159)	0.292 (1.170)	0.324 (1.144)	0.329 (1.153)
training	0.2	400	0.134 (1.204)	**0.333 (1.099)**	0.272 (1.161)	0.308 (1.144)	0.324 (1.144)	0.329 (1.153)
total	none[b]	1716	0.218 (1.226)	0.473 (1.014)	0.580 (0.913)	0.637 (0.856)	0.658 (0.838)	**0.681 (0.816)**
total	0.1	2625	0.282 (1.175)	0.510 (0.978)	0.594 (0.898)	0.590 (0.910)	0.617 (0.887)	**0.634 (0.874)**
total	0.2	1125	0.237 (1.211)	0.519 (0.969)	0.556 (0.939)	0.556 (0.946)	0.587 (0.921)	**0.608 (0.905)**
total	0.3	500	0.184 (1.252)	**0.492 (0.996)**	0.481 (1.015)	0.487 (1.017)	0.470 (1.042)	0.427 (1.093)

[a] The numbers in bold represent the q^2 values for the optimal number of components and the lowest SDEP. [b] The results of conventional CoMFA.

Table 4. Summary of CoMFA/q^2-GRS Results

	training set (compounds **1**−**47**)		total 66	
	conventional CoMFA	CoMFA/ q^2-GRS	conventional CoMFA	CoMFA/ q^2-GRS
q^2 threshold	none	0.1	none	0.1
minimum σ	2.0	2.0	2.0	2.0
no. of small boxes	none	7	none	22
no. of lattice points	1210	700	1716	2750
optimal no. of components	3	6	6	6
q^2	0.460	0.513	0.681	0.634
SDEP	1.031	1.113	0.816	0.874
SEE	0.337	0.372	0.347	0.388
R^2	0.941	0.928	0.941	0.927
F values	141.535[a]	114.096[a]	192.8[b]	151.848[b]
prob of $R^2 = 0$	0.000[a]	0.000[a]	0.000[b]	0.000[b]
relative contributions				
steric	0.648	0.553	0.663	0.635
electrostatic	0.352	0.447	0.337	0.365

[a] $n1 = 5$, $n2 = 44$. [b] $n1 = 5$, $n2 = 60$.

Scheme 1

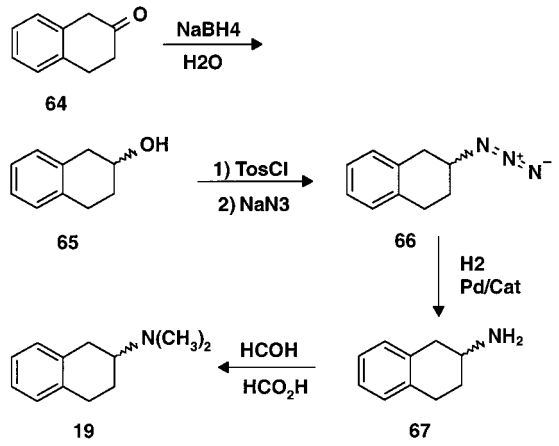

receptor affinity was measured in our laboratory. This data set includes a variety of *trans*- and *cis*-H_2-PAT analogues (Table 1), as well as representatives of several other structural classes (Chart 2, Table 2). The competition binding activity of the compounds is expressed as $-\log(K_{0.5})$ (Table 5). In the case of racemic mixtures, the affinity of the active enantiomer was approximated by dividing the $K_{0.5}$ by 2, making the assumption that one enantiomer was significantly less active than the other. For those compounds with chiral centers, racemic data was used and we modeled them as close as possible to (−)-*trans*-H_2-PAT. Compounds **26**, **27**, and **52** were modeled such that the 3-amino group had an (*S*) configuration; Compounds **42**, **47**, **48**, and **49** were modeled in the configurations shown in Chart 3. Since compounds **41**, **59**, and **63** are extremely flexible molecules, stereochemistry at the chiral centers matters little in alignment with (−)-*trans*-H_2-PAT. Enantiomers of these compounds were constructed, and configurations that best matched (−)-*trans*-H_2-PAT were used. The enantiomer of compound **46** used was the (*R*) configuration since it best matched (−)-*trans*-H_2-PAT. For all racemic *trans*-H_2-PAT analogues, (−)-*trans*-H_2-PAT was used as a template. For all racemic *cis*-H_2-PAT analogues, (−)-*cis*-H_2-PAT was used. Thus, this strategy is likely to be valid based on the available data with this receptor and compounds of the structural classes we used. Structure optimization and field fit minimization were performed using the standard Tripos force field with the maximum iteration cutoff of 1000 steps. SYBYL random search method was used to search for low-energy conformers. All calculations were performed on a Silicon Graphics Indigo2 workstation. The default SYBYL settings were used except where otherwise noted.

Structure Generation and Alignment Rules

We have analyzed the SARs for the total of 66 compounds that were initially separated into two groups: training set (compounds **1**−**47**) and test set (compounds **48**−**63**). The use of chemically diverse test compounds (as compared to the compounds in the training set) is generally recommended for assessing the true predictability of any QSAR study. The compounds in the training set consisted of a wide range of structures, including PATs and non-PAT molecules that exhibit a wide range of affinities. We also selected ligands that vary structurally and represent different receptor classes to form the test set.

The conformation of the template molecule, (−)-*trans*-H_2-PAT, was chosen from a previous modeling study of the PAT binding site.[16] All *trans*-PAT analogues were

Table 5. CoMFA Actual, Calculated, and Predicted Activities for Training and Test Set Molecules

		training set (**1**−**47**) or test set (**48**−**63**)								all compounds			
		conventional CoMFA				q^2-GRS cutoff = 0.1				conventional CoMFA		q^2-GRS cutoff = 0.1	
compd	actual	calcd	resid	pred	resid	calcd	resid	pred	resid	calcd	resid	calcd	resid
1a	9.48	9.06	0.42			9.56	−0.08			9.12	0.36	9.19	0.29
1b	7.87	7.93	−0.06			8.44	−0.57			7.70	0.17	8.09	−0.22
1c	8.54	8.50	0.04			9.01	−0.47			8.67	−0.13	8.79	−0.25
1d	7.15	7.38	−0.23			7.41	−0.26			7.11	0.04	7.46	−0.31
2	9.46	8.96	0.5			8.33	1.13			8.44	1.02	8.53	0.93
3	7.76	8.02	−0.26			8.42	−0.66			8.37	−0.61	8.52	−0.76
4	7.25	6.53	0.72			6.44	0.81			6.57	0.68	6.22	1.03
5	8.55	8.86	−0.31			8.61	−0.06			8.52	0.03	8.45	0.10
6	8.77	8.81	−0.04			8.93	−0.16			8.97	−0.20	8.97	−0.20
7	8.26	8.28	−0.02			8.32	−0.06			8.14	0.12	8.10	0.16
8	6.22	6.43	−0.21			6.61	−0.39			6.67	−0.45	6.59	−0.37
9	6.33	6.73	−0.4			6.81	−0.48			6.85	−0.52	6.86	−0.53
10	7.26	7.39	−0.13			7.19	0.07			6.98	0.28	7.35	−0.09
11	7.98	7.73	0.25			8.12	−0.14			7.74	0.24	7.99	−0.01
12	7.52	7.39	0.13			7.64	−0.12			7.39	0.13	7.32	0.20
13	8.32	8.3	0.02			8.27	0.05			8.22	0.10	8.28	0.04
14	8.04	8.56	−0.52			8.29	−0.25			8.52	−0.48	8.33	−0.29
15	9.02	8.46	0.56			8.60	0.42			8.17	0.85	8.27	0.75
16	7.15	6.93	0.22			7.03	0.12			7.23	−0.08	7.11	0.04
17	6.78	6.95	−0.17			7.10	−0.32			7.02	−0.24	7.27	−0.49
18	6.97	7.07	−0.1			7.13	−0.16			7.05	−0.08	7.22	−0.25
19	7.08	7.45	−0.37			6.76	0.32			7.24	−0.16	7.16	−0.08
20	7.58	7.53	0.05			7.37	0.21			7.51	0.07	7.37	0.21
21	8.29	8.61	−0.32			8.30	−0.01			8.45	−0.16	8.45	−0.16
22	8.35	8.98	−0.63			8.77	−0.42			8.35	0.00	8.79	−0.44
23	8.85	9.01	−0.16			8.99	−0.14			8.46	0.39	9.13	−0.28
24	9.12	8.86	0.26			8.58	0.54			8.34	0.78	8.58	0.54
25	7.23	6.93	0.3			7.13	0.10			7.16	0.07	7.1	0.13
26	5.32	5.44	−0.12			5.10	0.22			5.83	−0.51	5.66	−0.34
27	5.32	5.28	0.04			5.17	0.15			5.53	−0.21	5.30	0.02
28	9.6	9.68	−0.08			8.98	0.62			9.46	0.14	9.13	0.47
29	5.3	6.05	−0.75			5.71	−0.41			5.87	−0.57	6.04	−0.74
30	8.38	8.16	0.22			8.45	−0.07			8.09	0.29	8.24	0.14
31	7.35	7.24	0.11			7.42	0.23			7.60	0.05	7.49	0.16
32	5.9	5.8	0.1			5.93	−0.03			5.75	0.15	6.05	−0.15
33	6.12	5.6	0.52			5.87	0.25			5.85	0.27	5.90	0.22
34	5.3	5.62	−0.32			5.65	−0.35			5.42	−0.32	5.45	−0.15
35	6.20	6.60	−0.4			6.47	−0.27			6.52	−0.32	6.57	−0.37
36	8.39	7.93	0.46			8.52	−0.13			8.37	0.02	8.53	−0.14
37	6.83	6.82	0.01			6.88	−0.05			6.66	0.17	6.72	0.11
38	7.68	7.72	−0.04			8.19	−0.51			8.23	−0.55	8.16	−0.48
39	9.51	9.75	−0.24			9.48	0.03			9.75	−0.24	9.47	0.04
40	9.92	10.04	−0.12			9.71	0.21			9.95	−0.03	9.26	0.66
41	5.91	6.01	−0.1			5.92	0.01			6.01	−0.10	5.87	0.06
42	5.30	5.46	−0.16			5.30	0.00			5.53	−0.23	5.66	−0.36
43	10.22	10.07	0.15			9.85	0.37			10.16	0.06	10.19	0.03
44	9.07	8.87	0.2			9.12	−0.05			9.3	−0.23	9.04	0.03
45	8.24	8.21	0.03			8.05	0.19			8.32	−0.08	8.10	0.14
46	7.04	6.69	0.35			6.90	0.14			6.87	0.17	6.93	0.11
47	7.00	6.43	0.57			6.58	0.42			6.71	0.29	6.55	0.45
48	5.52			5.54	−0.02			5.22	0.30	5.35	0.17	5.29	0.23
49	5.60			6.14	−0.54			6.03	−0.43	5.26	0.34	5.14	0.46
50	9.30			9.38	−0.08			9.66	−0.36	9.78	−0.48	9.93	−0.63
51	7.34			7.16	0.18			6.61	0.73	7.46	−0.12	6.91	0.43
52	5.82			6.32	−0.5			5.96	−0.14	5.79	0.03	5.84	−0.02
53	6.67			6.13	0.34			5.78	0.89	6.52	0.15	6.31	0.36
54	5.70			5.66	0.04			5.27	0.43	5.72	−0.02	5.51	0.19
55	9.52			8.45	1.07			7.72	1.80	9.34	0.18	9.12	0.40
56	5.30			5.85	−0.55			4.62	0.68	5.40	−0.10	5.44	−0.14
57	6.57			6.05	0.52			7.22	−0.65	6.72	−0.15	7.05	−0.48
58	8.75			8.25	0.50			8.30	0.45	9.41	−0.66	9.25	−0.50
59	9.62			9.38	0.24			8.67	0.95	9.67	−0.05	9.28	0.34
60	9.24			9.13	0.11			8.34	0.90	9.31	−0.07	9.25	−0.01
61	8.03			8.42	−0.39			9.20	−1.17	8.08	−0.05	8.04	−0.01
62	7.82			6.68	1.14			6.87	0.95	7.48	0.34	8.05	−0.23
63	6.74			6.65	0.09			5.61	1.13	6.9	−0.16	6.78	−0.04

constructed by modification of (−)-*trans*-H_2-PAT. All *cis*-PAT analogues were constructed by modification of (−)-*cis*-H_2-PAT.

All non-PAT analogues were constructed de novo using the sketch option of the building component of SYBYL. Conformational databases were developed for all non-PAT ligands using the Random Search subroutine of SYBYL. In this case, the energy cutoff for conformers was designated as 10 kcal/mol above that of the lowest-energy conformer found. All compounds

Chart 3. Binding Modes of Aromatic Substituents

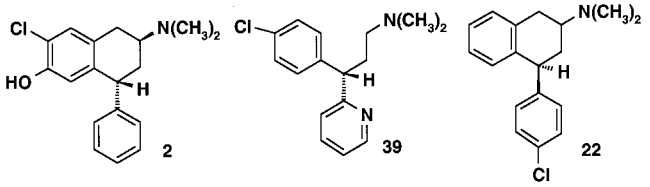

were modeled as the protonated cationic amines as these analogues exist primarily in this form at pH 7.4 and it is assumed that the cationic amine group acts as a hydrogen bond donor for the PAT binding site. Centroids were defined for each phenyl ring in order to obtain alignment of PAT and non-PAT analogues.

Structure Alignment. (−)-*trans*-H_2-PAT (**1a**) was used as a template onto which the PAT analogues, as well as **26** and **27**, were superimposed using SYBYL field fit routine. Centroids were defined for all aromatic rings of non-PAT compounds. The centroids and amine nitrogen of diphenhydramine (**36**), butaclamol (**37**), doxepin (**43**), mazindol (**46**), SCH-23390 (**47**), methysergide (**48**), SKF-8393 (**49**), amitriptyline (**50**), desipramine (**51**), haloperidol (**53**), mianserin (**55**), rimcazole (**56**), spiperone (**57**), ketanserin (**58**), promethazine (**59**), GBR-12909 (**61**), and nortriptyline (**62**) were superimposed with the corresponding structures of the template. Compounds **19**, (−)-NANM (**42**), and 7-OH-DPAT (**52**) were superimposed with the template using the protonated nitrogen, the centroid of the aromatic portion of the tetralin ring, and the C4 carbon with the C1 carbon of the template molecule and then field fitted to the template. Since (*R*)-chlorpheniramine (**38**) and (*S*)-chlorpheniramine (**39**) as well as *cis*- and *trans*-flupenthixol (**44** and **45**, respectively) have affinities similar to compounds **2** (Cl,OH-PAT) and **22** (*p*-Cl-PAT), respectively, **39** and **44** were aligned such that the substituted phenyl ring centroid superimposed with the centroid of the tetralin aromatic ring of the template. Compounds **38** and **45** were aligned such that the substituted phenyl ring centroid superimposed with the centroid of the pendant phenyl ring of the template. Triprolidine (**40**) and mepyramine (**60**) were superimposed such that the substituted phenyl ring is superimposed with the tetralin, since they have affinity similar to that of compound **2** as compared to **22**. The centroid of the atropine (**41**) phenyl ring was aligned with the centroid of the tetralin aromatic ring, the hydroxyl oxygen was fitted with the pendant phenyl ring centroid, and the two nitrogens were superimposed. Loperamide (**54**) was superimposed on compound **16**, a PAT with a phenylethyl substituent on the amine, which is structurally similar to **54**. BMY-14802 (**63**) was aligned such that the fluorophenyl ring centroid was superimposed on the template tetralin aromatic ring, the hydroxyl group with the pendant phenyl ring, and the piperizine ring with the tertiary amine.

Comparative Molecular Field Analysis. Conventional CoMFA was performed with the QSAR option of Sybyl. For each cross-validated CoMFA analysis, the minimum σ value was set to 2.0 to expedite calculations. The steric and electrostatic field energies were calculated using sp^3 carbon probe atoms with a +1 charge. The CoMFA grid spacing was 2.0 Å in the *x*, *y*, and *z* dimensions within the defined region, which extended beyond the van der Waals envelopes of all molecules by at least 4.0 Å. The CoMFA QSAR equations were calculated with the PLS algorithm as implemented in Sybyl. The optimal number of components in the final PLS model was determined by the standard error of prediction value obtained from the leave-one-out cross-validation technique.

q^2-GRS Routine.[23] A conventional CoMFA is performed initially using an automatically generated region file. The rectangular region grid encompassing aligned molecules is then broken into 125 small boxes of equal size, and the Cartesian coordinates of the upper-right lower-left corners of each box are calculated. The calculated coordinates are used to create region files with a +1 sp^3 C as a probe atom. For each of the newly created region files, a separate CoMFA is performed with a step size of 1 Å. The regions with a q^2 greater than a specified threshold are selected for further analysis and combined to generate a master region file. After the master region is generated, a final CoMFA is performed.

Results and Discussion

The affinities of PAT analogues for both the [^{3}H]-(−)-*trans*-H_2-PAT- and [^{3}H]mepyramine-labeled sites are shown in Table 1. We initially discuss the results of biological experiments followed by the analysis of molecular modeling studies.

Determination of the Requirement of the Pendant Phenyl Ring for *trans*-H_2-PAT Binding at the [^{3}H]-(−)-*trans*-H_2-PAT Binding Site. The majority of clinically useful H_1 antagonists contain a 1,1-diaryl-3-aminopropne moiety where the diaryl group is hypothesized to be a requirement for high affinity at the [^{3}H]mepyramine-labeled H_1 site.[24] In a study of triprolidine analogues, the replacement of one aryl group by hydrogen reduced antihistaminic activity.[10] To test the diaryl requirement at the [^{3}H]-(−)-*trans*-H_2-PAT site, compound **19** was synthesized and competition binding for both the [^{3}H]-(−)-*trans*-H_2-PAT- and [^{3}H]-mepyramine-labeled sites was evaluated (Table 2). Consistent with previous H_1 SAR studies that show the importance of a 1,1-diaryl moiety, compound **19** exhibits decreased affinity (∼100-fold) for both the [^{3}H]-(−)-*trans*-H_2-PAT-and [^{3}H]mepyramine-labeled sites, as compared to (±)-*trans*-H_2-PAT ($K_{0.5}$ = 1.4 and 1.1 nM, respectively). This indicates that the pendant phenyl ring is required for high-affinity binding at these two sites.

Effects of Substituents on the Aromatic Rings on [^{3}H]-(−)-*trans*-H_2-PAT Site Binding. Diaryl H_1 antagonists with a single *ortho*-substitution have been shown to possess decreased affinity for the [^{3}H]mepyramine-labeled sites. From a study of diphenhydramine analogues, it was determined that small lipophilic groups at the *ortho*-position reduced the antihistaminergic effects.[25] *o*-Methyl substitution on triprolidine's phenyl ring decreased affinity for the [^{3}H]mepyramine-labeled H_1 receptor by more than 1000-fold.[10] This decrease is believed to be due to a conformational change that disallows coplanarity of the diaryl ring system. To assess the effects of *ortho*-subsitution in the rigid (±)-*trans*-H_2-PAT, we synthesized *o*-chloro- and *o*-methyl-PATs with groups on the pendant phenyl ring.

The (±)-*o*-chloro-*trans*-H_2-PAT (**20**) has approximately 50-fold decreased affinity at both radiolabeled sites compared to (±)-*trans*-H_2-PAT (**1**), whereas the (±)-*o*-methyl-*trans*-H_2-PAT (**21**) has less than a 10-fold decrease in affinity (Table 1). The resultant decrease in affinity may be due to a compact hydrophobic pocket in the active sites that could not accommodate the *ortho*-substituent. The decrease in affinity of PATS with an *o*-chloro- or *o*-methyl substituent on the pendant phenyl ring also is consistent with the H_1-like characteristics of the [^{3}H]-(−)-*trans*-H_2-PAT site. The *ortho*-substituted PATs also possess decreased affinity for the [^{3}H]mepyramine-labeled H_1 receptor (Table 1), further indicating the similarity of these two radiolabeled sites. In comparison to the earlier reported effects of *ortho*-substitution of triprolidine, *o*-methyl substitution on the PAT nucleus only results in a 10-fold decrease at both the [^{3}H]-(−)-*trans*-H_2-PAT-and [^{3}H]mepyramine-labeled sites, indicating the relative positions of the ring systems in this rigid compound do not change significantly by this substituent.

Para-substitution on an aromatic ring of H_1 antagonists such as mepyramine (**60**), (+)-chlorpheniramine (**39**), and triprolidine (**40**) provides for high affinity for the [^{3}H]mepyramine-labeled H_1 receptor ($K_{0.5}$ = 0.58, 0.31, and 0.12 nM, respectively). However, *para*-substitution on the pendent phenyl ring of (±)-*trans*-H_2-PAT results in decreased affinity at both the [^{3}H]-(−)-*trans*-H_2-PAT- and [^{3}H]mepyramine-labeled sites (Table 1). The *p*-chloro-substituted PAT (**22**) has approximately 6-fold less affinity for the [^{3}H]-(−)-*trans*-H_2-PAT-labeled site as compared to (±)-*trans*-**1** and a similar decrease in affinity for the [^{3}H]mepyramine-labeled site. The (±)-*p*-methyl-substituted PAT (**23**) also exhibits a similar decrease in affinity at both radiolabeled sites. However, *p*-fluoro substitution (**24**) does not exhibit a decrease in affinity for these sites. Chlorine and methyl substituents have increased van der Waals radii as compared to hydrogen or fluorine; therefore the decrease in affinity of **22** and **23** may be due to increased steric bulk of their *para*-substituents.

Aromatic disubstituted H_1 ligands have not been analyzed previously at the [^{3}H]mepyramine-labeled site. Previously synthesized *trans*- and *cis*-6,7-Cl,OH-PAT analogues (**2** and **28**) bind with high affinity ($K_{0.5}$ = 0.63 and 0.5 nM, respectively, Table 1) to the [^{3}H]-(−)-*trans*-H_2-PAT site, whereas the *cis*- and *trans*-6,7-diOH-PAT analogues (**12** and **13**) have decreased affinity ($K_{0.5}$ = 9.6 and, 60 nM, respectively, Table 1). We now have analyzed competition binding studies for these compounds to assess the substituent effects on the [^{3}H]-mepyramine-labeled site. As indicated in Table 1, these compounds have nearly identical affinity for both radiolabeled sites. These results suggest that a 6-OH substituent, capable of forming hydrogen bonds, is detrimental to binding, while a 6-Cl group that is hydrophobic may be beneficial for binding at either radiolabeled site.

The novel rigid aromatic ring-substituted PAT compounds have provided important information regarding the way the [^{3}H]-(−)-*trans*-H_2-PAT- and [^{3}H]mepyramine-labeled sites accommodate aromatic ring substituents. (*S*)-Chlorpheniramine (**39**) and triprolidine (**40**) ($K_{0.5}$ = 0.31 and 0.12 nM, respectively), which have *para*-substituents on a phenyl ring can bind to the [^{3}H]-(−)-*trans*-H_2-PAT-labeled site in a fashion similar to the *para*-substituted PATs, but they bind with 10-fold higher affinity. However, the high binding affinity of chlorpheniramine and triprolidine correlates well with the observed affinity of the *trans*- and *cis*-6,7-Cl,OH-PAT analogues (**2** and **28**), which also have substituents on an aromatic ring. This correlates well with antihistaminergic studies of a series of diarylaminopropenes synthesized by Warringa et al.[11] They found that *para*-substitutions on the aromatic ring *cis* with respect to the amine increased antihistaminergic activity, while *para*-substitutions on the *trans* aromatic ring decreased the activity. Because of our studies with the rigid PATs, which lock the position of the amine in relation to the aryl ring, we propose that chlorpheniramine and similar molecules bind to both of the [^{3}H]-(−)-*trans*-H_2-PAT- and [^{3}H]mepyramine-labeled sites with their aryl ring substituents in the same molecular space as the tetralin aryl ring of *trans*-Cl,OH-PAT (**2**) (Chart 3).

Effects of Other Compounds on Binding at [^{3}H]-(−)-*trans*-H_2-PAT- and [^{3}H]Mepyramine-Labeled Sites. It is generally recognized that quaternary amino groups on ethylenediamine and aminoalkyl ethers decrease activity at the H_1 receptor.[26] Previous results[15] indicated that the racemic *trans*-cationic quaternary amine **3** possesses moderate (35 nM, Table 1) but significantly less affinity for the [^{3}H]-(−)-*trans*-H_2-PAT binding site as compared to (±)-*trans*-**1**. The decrease in affinity of **3** is believed to be due to inability to donate a hydrogen bond for high-affinity binding. Compound **3** also has diminished affinity for the [^{3}H]mepyramine-labeled sites (120 nM, Table 1). This suggests that the histamine H_1 receptor cannot accommodate a permanently charged PAT and that hydrogen bond donation is crucial for PAT binding at this site also. To test further if ability for hydrogen bond donation is a possible requirement for high-affinity binding and to test the effects of stereochemistry on permanently charged PATs at these two sites, we synthesized compound **25**, the quaternary amine analogue of (±)-*cis*-H_2-PAT. Like *trans*-cationic quaternary amine **3,** compound **25** exhibits a decrease in affinity for both the [^{3}H]-(−)-*trans*-H_2-PAT- and [^{3}H]mepyramine-labeled sites, further suggesting the importance of hydrogen bond donation.

For maximal H_1 antagonist activity, the aromatic rings of diphenhydramine cannot be coplanar. The fluorene analogue of diphenhydramine, which forces both rings to be coplanar, is 100 times less active.[27] In potent phenothiazine H_1 antagonists (promethazine, **59**), the tricyclic ring system is not coplanar because the thiazine ring is in the boat conformation. To test the effects of a coplanar ring system on binding at the [^{3}H]-(−)-*trans*-H_2-PAT- and [^{3}H]mepyramine-labeled sites, we analyzed 3-aminofluoranthene (**26**) and its dimethylated analogue (**27**). These compounds have decreased and identical affinity at the two sites. The decrease in affinity can be due to coplanarity of the ring systems, consistent with previous literature, or to the change of the relative position of the amine as compared to (±)-**1**.

All the proposed analogues in this study possess nearly equal affinity for the [^{3}H]-(−)-*trans*-H_2-PAT- and [^{3}H]mepyramine-labeled sites; therefore, we analyzed

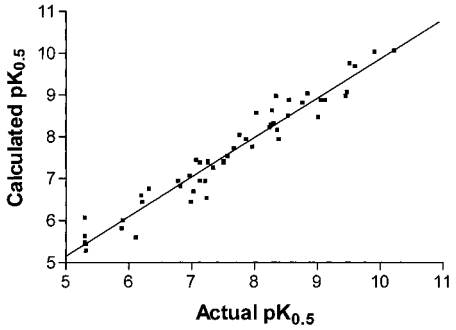

Figure 1. Actual versus calculated p$K_{0.5}$ for the training set (**48**−**63**) using conventional CoMFA (cf. Table 5).

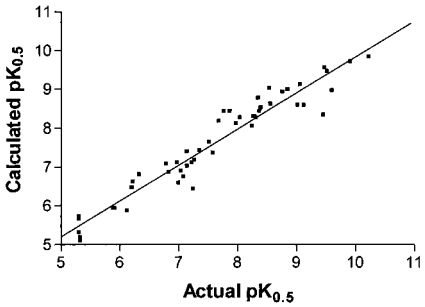

Figure 2. Actual versus calculated p$K_{0.5}$ for all compounds using q^2-GRS (cf. Table 5).

a number of previously synthesized PAT analogues and non-PAT compounds at the [^{3}H]mepyramine-labeled sites to identify possible differences in the SAR of the radiolabeled sites. As indicated in Tables 2 and 3, none of the tested PAT analogues nor non-PAT ligands are able to distinguish strongly (difference in $K_{0.5}$ between [^{3}H]-(−)-*trans*-H_2-PAT- and [^{3}H]mepyramine-labeled sites is less than 5-fold) between these two radiolabeled sites. Also, (−)-*trans*-H_2-PAT (**1a**) and mepyramine have the same affinity at each radiolabeled site (Table 2). This leads us to believe that both radioligands label histamine H_1 receptors with the same SAR in rodent brain. Therefore, we believe that a CoMFA model of the [^{3}H]-(−)-*trans*-H_2-PAT site is an important representation of binding to histamine H_1-type receptors in mammalian brain.

CoMFA and CoMFA/q^2-GRS of Ligands Included in the Training Set. The results obtained after performing CoMFA/q^2-GRS are summarized in Table 3. The training set (compounds **1**−**47**) was assessed initially by conventional CoMFA. The q^2-GRS routine[23] was then applied to optimize the standard CoMFA model. Initial conventional CoMFA produced a q^2 of 0.460 and standard error of prediction (SDEP) of 1.031 with 3 components. (Table 3) Various q^2 threshold values were tried to remove irrelevant variables (noise). The highest q^2 value (0.513, 6 components) and lowest SDEP value (0.982) were obtained with the q^2 threshold value of 0.1. Since the q^2 values associated with conventional CoMFA and q^2-GRS were similar, we used both methods for subsequent non-cross-validated PLS runs. This yielded a conventional R^2 of 0.941 and a standard error of estimate (SEE) of 0.337 for the conventional CoMFA and a conventional R^2 of 0.928 and a SEE of 0.372 for q^2-GRS (Table 4). Using these PLS models, the activity of each compound was calculated and compared with the actual value (Figures 1and 2). It was found that overall the residuals were low. The compounds with the

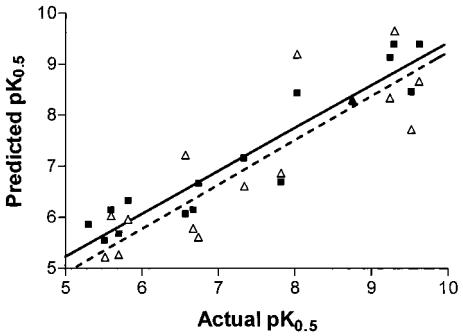

Figure 3. Actual versus *predicted* p$K_{0.5}$ of test set molecules (**1**−**47**): ■ and solid line, conventional CoMFA; △ and dashed line, q^2-GRS; R^2 (conventional CoMFA) = 0.8943, R^2 (q^2-GRS) = 0.7712.

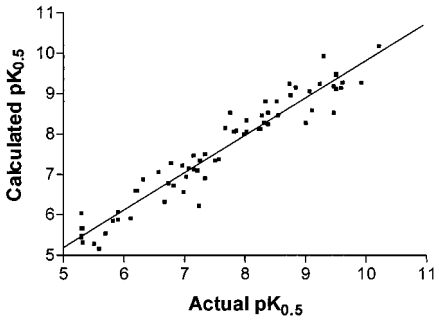

Figure 4. Actual versus calculated p$K_{0.5}$ for all compounds using conventional CoMFA (cf. Table 5).

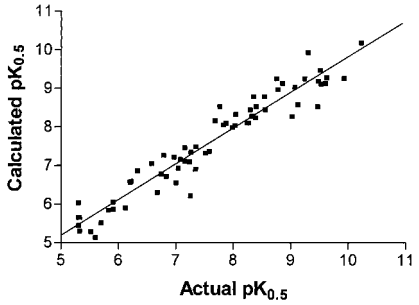

Figure 5. Actual versus calculated p$K_{0.5}$ for all compounds using q^2-GRS (cf. Table 5).

worst residuals for conventional CoMFA were **29** and **4** (−0.75 and 0.72, respectively) and **2** and **4** (1.13 and 0.81, respectively) for q^2-GRS. The poor prediction of **4** by both models is surprising considering that other secondary amine PATs (**30**−**33**) were predicted with low residuals by both models. The high residual (underprediction of affinity) for **2** obtained from the q^2-GRS model is most likely due to an overwhelming amount of compounds in the model with similar substitution patterns that have low affinity. For example, **12**, **13**, **29**, **34**, and **47** all have an equivalent 7-hydroxyl group but all have greater than 100-fold less affinity for the binding site.

CoMFA/q^2-GRS of Ligands Included in the Test Set. The PLS models obtained for the conventional and q^2-GRS were used to predict the activities of 16 compounds included in the test set. The predicted activities for compounds **48**−**63** are shown in Table 5, and the plot of actual versus predicted activities for both prediction methods are shown in Figure 3. Predictive R^2 of 0.8943 for conventional CoMFA and 0.7712 for q^2-GRS were obtained for the test set. This result is somewhat

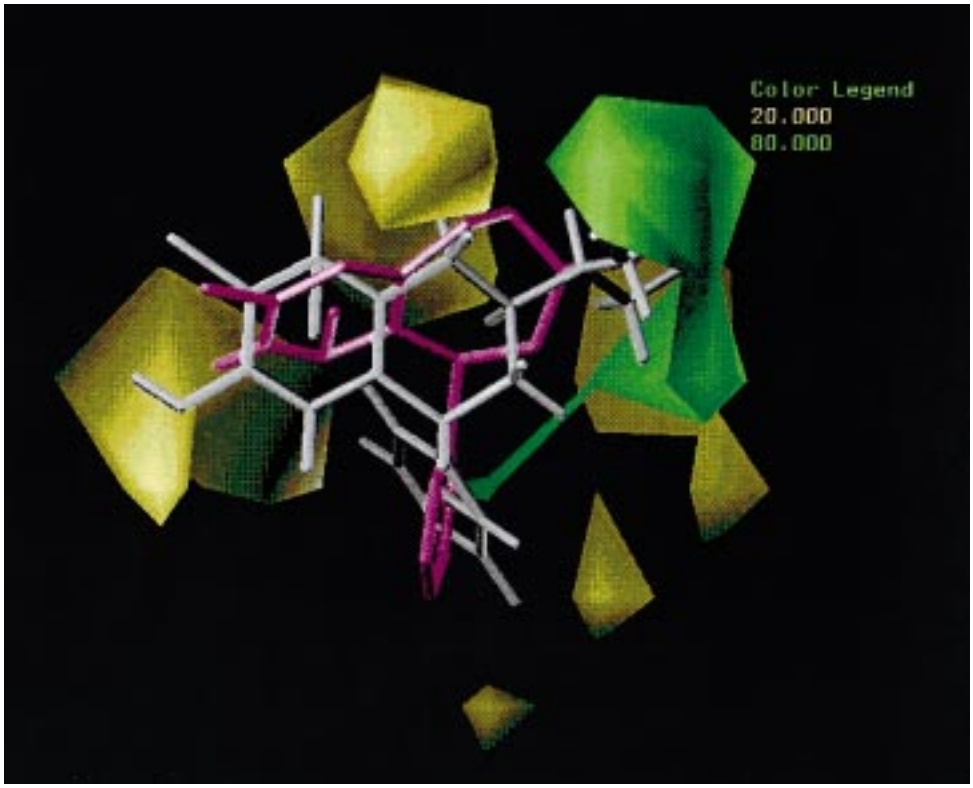

Figure 6. CoMFA steric stdev*coeff contour plot. Green regions represent a contribution level of 80%, i.e., sterically favored areas. Yellow regions represent a contribution level of 20%, i.e., sterically disfavored areas. Compounds **2** and **47** are depicted in white and magenta, respectively.

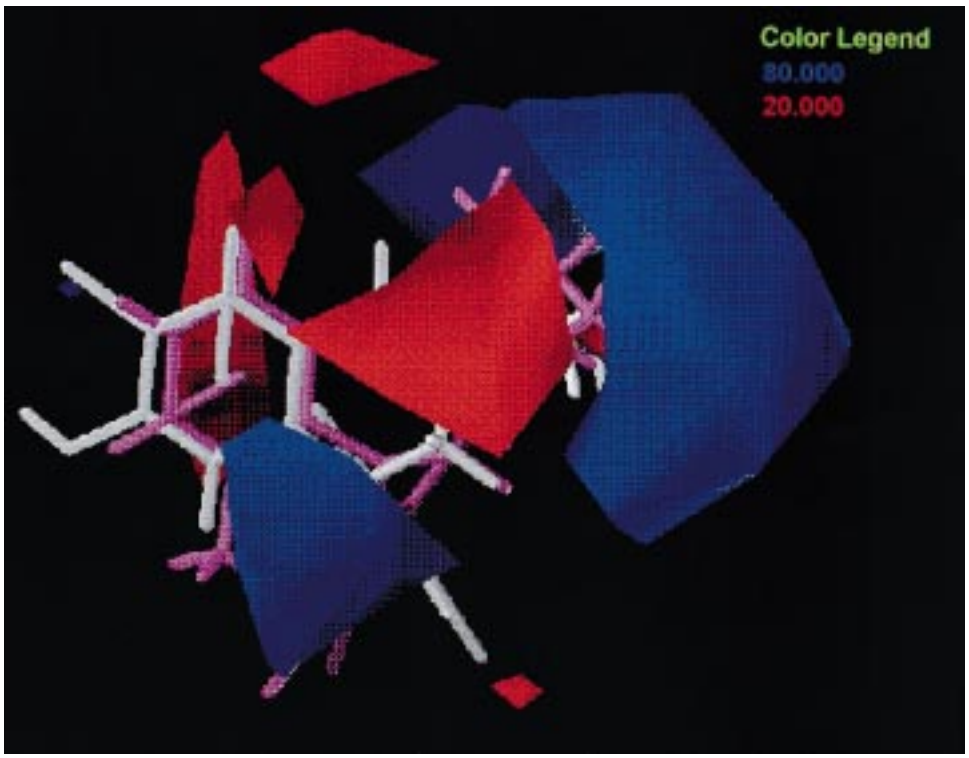

Figure 7. CoMFA electrostatic stdev*coeff contour plot. Blue regions represent a contribution level of 80%, i.e., positive charge favored areas. Red regions represent a contribution level of 20%, i.e., positive charge disfavored areas. Compounds **2** and **43** are depicted in white and magenta, respectively.

surprising because the q^2 for the training set obtained by q^2-GRS is higher than that for conventional CoMFA (Table 3). Thus, q^2-GRS results in a higher q^2 while exhibiting decreased external predictability as evidenced by the test set. This could be due to the fact that q^2-GRS as a variable selection procedure may have a tendency to overfitting as was noticed recently by Ortiz et al.,[28] which results in better internal q^2 but lower external R^2 than those obtained with conventional CoMFA

Due to the better predictability of conventional CoMFA model, we hypothesized that it may represent steric and electrostatic fields important to binding at the [^{3}H]-*trans*-H_2-PAT site. Since this model predicted the test set well (compounds **48**−**63**), we added these compounds to the training set to obtain a total of 66 compounds. The results of conventional CoMFA and q^2-GRS with different cutoffs are shown in Table 3. Initial conventional CoMFA (sp^3 carbon with a +1 charge) gave a q^2 of 0.681 and SDEP of 0.816 at 6 components, while q^2-GRS with 0.1 as a cutoff gave a q^2 of 0.635 and SDEP of 0.874 at 6 components. Since both models resulted in a high q^2, we used these analyses to obtain non-cross-validated CoMFA results as indicated in Table 4 (conventional CoMFA, $R^2 = 0.941$, SEE = 0.347, $F = 192.8$; q^2-GRS, $R^2 = 0.927$, SEE = 0.388, $F = 151.85$). The actual, calculated, and residual activities for both CoMFA methods are shown in Table 5. The plot of actual versus calculated activities is shown in Figures 4and 5.

CoMFA Fields. The CoMFA steric and electrostatic fields obtained from the conventional CoMFA and the structures of sample ligands are shown in Figures 6 and 7, respectively. The field values were calculated by multiplying the β coefficient and standard deviation of columns in the QSAR table (stdev*coeff). The green (sterically favorable) and yellow (sterically unfavorable) contours shown in Figure 6 represent 80% and 20% level contributions, respectively. The green contour region adjacent to the amine of **2** indicates that a dimethyl substitution pattern is optimal for binding at this radiolabeled site. The yellow contour regions at the 2 and 4 carbons indicate that steric bulk is not well-accommodated by the site on these areas of the PAT nucleus. The 8-hydroxy group on **47** extends into a yellow contour region that signifies that steric bulk is not well-accommodated by the site. Overall, the steric contour regions well-represent binding of molecules at the [^{3}H]-(−)-*trans*-H_2-PAT binding site.

The contours generated using the electrostatic field are displayed in Figure 7. The blue (positive charge favorable) and red (positive charge disfavorable) contours represent 80% and 20% level contributions, respectively. The red contour regions indicate that positive charge of amino groups on the C2 or C4 position of the PAT nucleus is not well-accommodated by the site. Since many compounds with hydroxyl substituents bind with low affinity (due to either hydrogen bond donor or acceptor properties) we would have expected a red contour adjacent to the 7-hydroxy group of **2.** With the poor prediction of **2**, as described for both the training set and final models, we should now design ligands that more effectively probe this area of the pharmacophore.

This model represents improvements on our previously published model in a number of ways: an increased number of compounds was used for the CoMFA, to 66 up from 35; a greater majority of rigid molecules have been used to define a training set for analysis; and a test set was used to validate our initial model of 50 compounds. As discussed above, 33 of these compounds have been tested at the [^{3}H]mepyramine-labeled H_1 binding site. Since these compounds have nearly identical affinity at the two radiolabeled sites, and we believe that the two sites are identical, this model represents binding at the known H_1 receptor. Therefore, this model can be used also to predict high-affinity ligands for the [^{3}H]mepyramine-labeled H_1 binding site.

Experimental Section

All chemicals were used as received from the manufacturers. Melting points were determined on a Mel-temp apparatus and are uncorrected. Proton NMR spectra were obtained in $CDCl_3$ (unless noted otherwise) using a Bruker AC300 300-MHz spectrometer. Elemental compositions (C, H, and N) of test compounds were determined by MHW Laboratories (Phoenix, AZ) and agreed with calculated values ±0.4%. Gas chromatographic analysis was performed using a Shimadzu GC-8A chromatograph with 2.0-m column packed with 3% OV-17 on chromasorb. Thin-layer chromatography was performed using silica gel 60 coated glass plates (Fisher Scientific), and column chromatography was performed with silica gel 60 (70−230 mesh). The starting compound for the synthesis of the 1-phenyl-3-amino-1,2,3,4-tetrahydronaphthalenes consisted of 1-phenyl-2-propanol which was obtained from Aldrich Chemical Co. Oxidation of 1-phenyl-2-propanol with pyridinium chlorochromate gave phenylacetone in approximately 70% yield.

2-Hydroxy-1,2,3,4-tetrahydronaphthalene (65). To a stirred slurry of $NaBH_4$ (2.6 g, 68.5 mmol) in 50 mL of MeOH was added dropwise a solution of β-tetralone (**64**) (5.0 g, 34.2 mmol) in MeOH. The reaction was refluxed for 4 h, and volatiles were evaporated in vacuo. H_2O (100 mL) was added and extracted with CH_2Cl_2, which was evaporated in vacuo. Column chromatography (CH_2Cl_2) afforded 2.82 g (56%) of a bright red oil: ^{1}H NMR ($CDCl_3$) δ 1.8 (m, 1H, CH), 2.1 (m, 1H, CH), 2.7 (d of d, 1H, CH), 3.0 (m, 2H, CH_2), 3.1 (d of d, 1H, CH), 4.3 (m, 1H, CHOH), 7.15 (s, 4H, ArH_4).

2-Azido-1,2,3,4-tetrahydronaphthalene (66). The 2-hydroxy-1,2,3,4-tetrahydronaphthalene (**65)** (2.82 g, 19.1 mmol) was dissolved in dry pyridine, and *p*-toluenesulfonyl chloride (7.2 g, 38.1 mmol) in pyridine was added. The solution was kept at 4 °C for 2 weeks. The solution was poured into ice water, filtered, and yielded a gray white precipitate which was dried in vacuo to afford 5.9 g (>100% of product). To a solution of 2-tosyloxy-1,2,3,4-tetrahydronaphthalene (5.9 g, 19.6 mmol) in 10 mL of dimethylformamide was added dropwise a solution of sodium azide (2.6 g, 40 mmol) in 10 mL of water. The reaction was heated to 45−50 °C and stirred for 4 h. The solution was poured into ice water and extracted with CH_2Cl_2. The organic layer was evaporated in vacuo to afford 3.2 g (94%) of a brown-gray oil.

2-Amino-1,2,3,4-tetrahydronaphthalene (67). The previous azide (**66**) (3.2 g,18.5 mmol) was dissolved in 200 mL of 2-propanol and shaken on a Parr hydrogenation apparatus over 150 mg of 5% Pd/C at 50 psi overnight. The catalyst was filtered and the filtrate evaporated in vacuo to yield 0.9 g of a green oil. Column chromatography with CH_2Cl_2:methanol (9:1) afforded 140 mg (0.95 mmol, 5.1%) of a yellow-brown oil: ^{1}H NMR ($CDCl_3$) δ 1.7 (m, 1H, CH), δ 2.1 (m, 1H, CH), 2.6 (d of d, 1 H, CH), 2.9 (m, 2H, CH_2), 3.1 (d of d, 1H, CH), 3.2 (m, 1H, CHN), 7.1 (s, 4H, ArH_4).

2-(*N,N*-Dimethylamino)-1,2,3,4-tetrahydronaphthalene Hydrochloride Salt (19). The primary amine (**67**) (137 mg, 0.93 mmol) was dissolved in 2 mL of 37% formaldehyde and 3 mL of 96% formic acid and refluxed for 4 h. The volatiles were removed in vacuo, and the salt was dissolved in water. This was extracted with methylene chloride, and the organic layer separated and evaporated to yield 139 mg of a brown oil. Column chromatography with CH_2Cl_2:methanol (9:1) afforded 77 mg (50%) of a light brown oil. This was dissolved in ethereal HCl, and the salt recrystallized from ethanol to afford 15 mg (16%) of colorless crystals: mp 211−212 °C; ^{1}H NMR ($CDCl_3$) δ 1.7 (m, 1H, CH), δ 2.1 (m, 1H, CH), 2.4 (s, 6H, $N(CH_3)_2$) 2.6 (d of d, 1 H, CH), 2.9 (m, 2H, CH_2), 3.1 (d of d, 1H, CH), 3.2 (m, 1H, CHN), 7.1 (s, 4H, ArH_4). Anal. ($C_{12}H_{18}NCl$) C,H.

1-(2-Chlorophenyl)-4-phenyl-1-buten-3-one (68). General Procedure. This intermediate was prepared from 2-chlorobenzaldehyde and phenylacetone by the method of South-

wick et al.[29] in 72% yield as a crude brown oil (21 g) estimated as 60% pure by gas chromatography, and used unpurified in next synthetic step.

1-(2-Methylphenyl)-4-phenyl-1-buten-3-one (69). A solution of 2-CH_3-bendzaldehyde and phenylacetone was reacted as above to afford 19 g of a viscous oil in 79% yield: ^{1}H NMR ($CDCl_3$) δ 7.2−7.85 (m, 9H, ArH), 6.7 (d, 1H, styryl), 3.7 (d, 1H, styryl), 4.0 (s, 2H, CH_2), 2.4 (s, 3H, CH_3).

1-(4-Chlorophenyl)-4-phenyl-1-buten-3-one (70). This intermediate was prepared as above in 31% yield as a white solid from phenyl acetone and 4-chlorobenzaldehyde: mp 132−138 °C; ^{1}H NMR ($CDCl_3$) δ 7.2−7.85 (m, 9H, ArH), 7.0 (d, 1H, styryl), 6.6 (d, 1H, styryl), 4.2 (s, 2H, CH_2).

1-(4-Methylphenyl)-4-phenyl-1-buten-3-one (71). This intermediate was prepared as above in 6.9% (1.7 g) yield as white solid estimated as 90% pure and used unpurified in the next synthetic step: ^{1}H NMR ($CDCl_3$) δ 7.6 (d, 1H, ArH), 7.5 (m, 2H, ArH), 7.25−7.4 (m, 5H, ArH), 7.05−7.15 (t, 2H, styryl, ArH), 6.7 (d, 1H, styryl), 3.95 (s, 2H, CH_2), 2.4 (s, 1H, $PhCH_3$).

1-(4-Fluorophenyl)-4-phenyl-1-buten-3-one (72). This intermediate was prepared as above in 35% (6.8 g) yield as yellow crystals: mp 78−79 °C; ^{1}H NMR ($CDCl_3$) δ 7.6 (d, 1H, ArH), 7.5 (m, 2H, ArH), 7.25−7.4 (m, 5H, ArH), 7.05−7.15 (t, 2H, styryl, ArH), 6.7 (d, 1H, styryl), 3.95 (s, 2H, CH_2).

1-(2-Chlorophenyl)-3-oxo-1,2,3,4-tetrahydronaphthalene (73). General Procedure. Compound **68** (21 g, impure) was dissolved in 700 mL of xylenes and added to a mechanically stirred suspension of polyphosphoric acid in 240 mL of xylenes. The reaction was heated to reflux for 7 h and monitored by gas chromatography. The xylenes were decanted, and the product was evaporated in vacuo to afford a crude red oil (18.1 g) that was immediately carried through to the next step without purification.

1-(2-Methylphenyl)-3-oxo-1,2,3,4-tetrahydronaphthalene (74). Compound **69** was prepared as above to afford 20 g of a dark amber oil. Chromatography of this oil on 400 g of silica gel (70−230 mesh) with toluene afforded 5.7 g (32%) of a viscous oil.

1-(4-Chlorophenyl)-3-oxo-1,2,3,4-tetrahydronaphthalene (75). Compound **70** (10.8 g, 42 mmol) was cyclized as above to afford a crude brown oil (15.5 g, 150%) that was immediately carried through to the next step without purification.

1-(4-Methylphenyl)-3-oxo-1,2,3,4-tetrahydronaphthalene (76). Compound **71** (1.7 g 7.2 mmol) was ring-closed as above to afford a yellow oil (2.0 g, 118%) that was immediately carried through to the next step without purification.

1-(4-Fluorophenyl)-3-oxo-1,2,3,4-tetrahydronaphthalene (77). Compound **72** (6.8 g, 28 mmol) was ring-closed as above to afford 6.8 g (100%) of an orange oil: ^{1}H NMR ($CDCl_3$) δ 7.0−7.4 (m, 9H, ArH), 4.1 (t, 1H, PhCHPh), 2.9 (m, 2H, $PhCH_2$), 2.3 (m, 2H, CH_2).

(±)-*cis*-1-(2-Chlorophenyl)-3-hydroxy-1,2,3,4-tetrahydronaphthalene (78). General Procedure. The crude tetralone **73** (70 mmol) was dissolved in MeOH, and $NaBH_4$ (247 mmol) was added in portions. The reaction was stirred magnetically and refluxed overnight. Cautiously, 100 mL of H_2O was added to the reaction. The volatiles were evaporated in vacuo. The residue was dissolved in CH_2Cl_2, extracted with water, dried over sodium sulfate, and evaporated in vacuo to afford 18 g of a crude orange oil. Column chromatography over silica gel (CH_2Cl_2) afforded 4.5 g (25%) of a yellow-brown gum: ^{1}H NMR ($CDCl_3$) δ 7.3−7.4 (m, 4H, ArH), 7.2−7.3 (m, 4H, ArH), 4.8 (dd, 1H, PhCHPh), 3.2 (dd, H, CHOH), 2.9 (m, 1H, $PhCH_2$), 2.9 (m, 1H, $PhCH_2$), 2.5 (m, 1H, CH_2), 2.0 (m, 1H, CH_2).

(±)-*cis*-1-(2-Methylphenyl)-3-hydroxy-1,2,3,4-tetrahydronaphthalene (79). Tetralone **74** (5.7 g (0.02 mol) was reduced as above to afford 5.0 g (88%) of semisolid.^{1}H NMR ($CDCl_3$) δ 7.0−7.3 (m, 8H, ArH), 4.4 (dd, 1H, PhCHPh), 4.3 (m, 1H, CHOH), 3.2 (m, 2H, $PhCH_2$), 2.9 (m, 2H, CH_2), 2.4 (s, 3H, CH_3).

(±)-*cis*-1-(4-Chlorophenyl)-3-hydroxy-1,2,3,4-tetrahydronaphthalene (80). Tetralone (**75**) (42 mmol) was reduced as above to afford 15 g of a crude orange oil. Column chromatography over silica gel (CH_2Cl_2) afforded 3.0 g (28%) of a pale yellow solid: mp: 97−105 °C; ^{1}H NMR ($CDCl_3$) δ 7.3−7.4 (m, 4H, ArH), 7.2−7.3 (m, 4H, ArH), 4.1 (dd, 1H, PhCHPh), 3.2 (m, 1H, CHOH), 2.9 (m, 2H, $PhCH_2$),2.4 (m, 2H, CH_2).

(±)-*cis*-1-(4-Methylphenyl)-3-hydroxy-1,2,3,4-tetrahydronaphthalene (81). Tetralone **76** (7.2 mmol) was reduced as above to afford 1.7 g of a crude orange oil. Column chromatography over silica gel (CH_2Cl_2) afforded 610 mg (35.6%) of a yellow-orange gum: ^{1}H NMR ($CDCl_3$) δ 6.9−7.2 (m, 8H, ArH), 4.15 (dd, 1H, PhCHPh), 3.2 (m, 1H, CHOH), 2.9 (m, 2H, $PhCH_2$), 2.4 (m, 2H, CH_2), 2.35 (s, 3H, Ph-CH_3).

(±)-*cis*-1-(4-Fluorophenyl)-3-hydroxy-1,2,3,4-tetrahydronaphthalene (82). The crude tetralone **77** (6.8 g, 28 mmol) was reduced as above to afford 4.0 g of a crude orange oil. Column chromatography over silica gel (CH_2Cl_2) afforded 2.1 g (31%) of a yellow wax: mp 83−86 °C; ^{1}H NMR ($CDCl_3$) δ 7.15−7.2 (m, 4H, ArH), 6.9−7.1 (m, 4H, ArH), 4.1 (dd, 1H, PhCHPh), 3.2 (m, 1H, CHOH), 2.9 (m, 2H, $PhCH_2$), 2.4 (m, 2H, CH_2).

(±)-*trans*-1-(2-Chlorophenyl)-3-azido-1,2,3,4-tetrahydronaphthalene (83). General Procedure. A solution of 7.2 g (38 mmol) of *p*-toluenesulfonyl chloride in 69 mL of dry pyridine was added to a solution of 4.45 g of alcohol **78** (17.2 mmol) in 69 mL of dry pyridine. The reaction was allowed to stand for 10 days at 4 °C and was then poured into ice water with stirring. The resulting light purple gum was filtered, dissolved in Et_2O, and extracted with 1 N HCl. The solvent was dried (Na_2SO_4) and evaporated in vacuo to afford 5.0 g (12.1 mmol, 70%) of the tosylate. A solution of sodium azide (2.0 g, 30.3 mmol) in 4.4 mL of water was added to the crude tosylate in DMF (33 mL). The reaction was stirred at 50 °C for 4.5 h. TLC (toluene) indicated complete reaction. The solution was poured into ice water and extracted with Et_2O. The organic layer was evaporated in vacuo to near dryness, and the solution was used immediately in the next synthetic step.

(±)-*trans*-1-(2-Methylphenyl)-3-azido-1,2,3,4-tetrahydronaphthalene (84). The alcohol **79** (5.0 g, 0.022 mol) was converted to the azide as above to afford 4.0 g (83%) of a gum that was used immediately in the next synthetic step.

(±)-*trans*-1-(4-Chlorophenyl)-3-azido-1,2,3,4-tetrahydronaphthalene (85). The alcohol **80** (3.0 g,11.6 mmol) was converted to the azide as above. The organic layer was evaporated in vacuo to near dryness, and the solution was used immediately in the next synthetic step.

(±)-*trans*-1-(4-Methylphenyl)-3-azido-1,2,3,4-tetrahydronaphthalene (86). The alcohol **81** (610 mg, 2.52 mmol) was converted to the azide as above. The organic layer was evaporated in vacuo to near dryness, and the solution was used immediately in the next synthetic step without purification.

(±)-*trans*-1-(4-Fluorophenyl)-3-azido-1,2,3,4-tetrahydronaphthalene (87). Alcohol **82** (2.1 g, 11.6 mmol) was converted to the azide as above and was used immediately in the next synthetic step.

(±)-*trans*-1-(2-Chlorophenyl)-3-amino-1,2,3,4-tetrahydronaphthalene (88). General Procedure. The azide **83** was dissolved in 200 mL of 2-propanol and shaken on a Parr hydrogenation apparatus over 100 mg of 10% Pd/C at 50 psi for 2 days. The catalyst was filtered, and the filtrate evaporated in vacuo to yield 3.2 g of a brown oil. Column chromatography with CH_2Cl_2:MeOH (90:10) afforded 700 mg (2.7 mmol, 22% from tosylate) of a light brown oil: ^{1}H NMR ($CDCl_3$) δ 7.4 (dd, 1H, ArH), 7.1−7.2 (m, 5H, ArH), 6.9 (d, 1H, ArH), 6.6 (dd, 1H, ArH), 4.7 (t, 1H, PhCHPh), 3.2 (m, 1H, PhCH), 3.1 (dd, 1H, PhCH), 2.6 (m, 1H, CH_2), 2.0 (m, 1H, CH_2), 1.6 (s, 2H, NH_2).

(±)-*trans*-1-(2-Methylphenyl)-3-amino-1,2,3,4-tetrahydronaphthalene (89). A solution of the azide **84** (4.0 g, 0.015 mol) in 150 mL of 2-propanol was hydrogenated as above to afford a gum which was purified by column chromatography (CH_2Cl_2: CH_2Cl_2−methanol (9:1)) to afford 2.3 g (66%) of a semisolid.

(±)-*trans*-1-(4-Chlorophenyl)-3-amino-1,2,3,4-tetrahydronaphthalene (90). The azide **85** was dissolved in 200 mL of 2-propanol and hydrogenated as above to afford 1.7 g of a crude green oil. Column chromatography with CH_2Cl_2:MeOH (95:5) afforded 1.3 g (5 mmol, 75% from tosylate) of a pale yellow oil.

(±)-*trans*-1-(4-Methylphenyl)-3-amino-1,2,3,4-tetrahydronaphthalene (91). The azide **86** was dissolved in 100 mL of 2-propanol and hydrogenated as above to yield 250 mg of a green oil. Column chromatography with CH_2Cl_2:MeOH (90:10) afforded 184 mg (0.78 mmol, 34% from tosylate) of a pale green oil: ^{1}H NMR ($CDCl_3$) δ 7.0−7.2 (m, 5H, ArH), 6.95 (d, 1H, ArH), 6.85 (dd, 1H, ArH), 4.3 (t, 1H, PhCHPh), 4.2 (dd, 1H, PhCH), 3.2 (m, 1H, PhCH), 2.8 (m, 1H, CHN), 2.3 (s, 3H, $PhCH_3$), 2.1 (s, 2H, NH_2), 2.1 (t, 1H, CHCN).

(±)-*trans*-1-(4-Fluorophenyl)-3-amino-1,2,3,4-tetrahydronaphthalene (92). The azide **87** was dissolved in 100 mL of 2-propanol and hydrogenated as above to yield 660 mg of a crude orange oil. Column chromatography with CH_2Cl_2:MeOH (95:5) afforded 356 mg (1.48 mmol, 22% from tosylate) of a pale yellow oil: ^{1}H NMR ($CDCl_3$) δ 7.05−7.2 (m, 4H, ArH), 6.85−7.0 (m, 4H, ArH), 4.4 (t, 1H, PhCHPh), 3.3 (m, 1H, PhCH), 3.2 (dd, 1H, PhCH), 2.9 (m, 1H, CH_2), 2.75 (m, 1H, CH_2), 2.1 (s, 2H, NH_2).

(±)-*trans*-1-(2-Chlorophenyl)-3-(*N*,*N*-dimethylamino)-1,2,3,4-tetrahydronaphthalene (20). General Procedure. The primary amine **88** (0.7 mg, 2.72 mmol) was dissolved in 7 mL of 37% formaldehyde and 10.5 mL of 96% formic acid and refluxed for 4 h. The volatiles were removed in vacuo, and the salt was partitioned between saturated $NaHCO_3$ and CH_2Cl_2 and the organic layer separated and evaporated in vacuo to afford 0.8 g (97%) of a brown oil which was dissolved in ethereal HCl and the salt recrystallized from ethanol to afford 100 mg (0.31 mmol) of white crystals: mp 209−210 °C; ^{1}H NMR ($CDCl_3$) δ 7.4 (dd, 1H, ArH), 7.0−7.2 (m, 5H, ArH), 6.9 (d, 1H, ArH), 6.65 (dd, 1H, ArH), 4.4 (t, 1H, PhCHPh), 3.1 (dd, 1H, PhCH), 2.9 (dd, 1H, PhCH), 2.6 (m, 1H, CHN), 2.3 (s, 6H, $N(CH_3)_2$), 2.1 (t, 1H, CHCN). Anal. ($C_{18}H_{21}NCl_2$) C,H,N.

(±)-*trans*-1-(2-Methylphenyl)-3-(*N*,*N*-dimethylamino)-1,2,3,4-tetrahydronaphthalene (21). The primary amine **89** (2.3 g, 98 mmol) was dimethylated as above. The semisolid was converted to the HCl salt with ethereal HCl as a methanol solution. The solution was stripped and the 2.5 g (100%) of residue dissolved in 5 mL of absolute ethanol and stored at −10 °C. Crystallization began, and a small amount of ether was added and the product again stored at −10 °C. Removal of the supernatant and drying afforded 1.1 g (37%) of a light yellow solid: mp 220−222 °C; ^{1}H NMR ($CDCl_3$) δ 7.3 (s, 1H, ArH), 7.2 (t, 2H, ArH), 7.1 (dd, 2H ArH), 6.85 (d, 1H, ArH), 6.6 (dd, 1H, ArH), 4.6 (t, 1H, PhCHPh), 3.1 (dd, 1H, PhCH), 2.9 (dd, 1H, PhCH), 2.6 (m, 1H, CHN), 2.45 (s, 3H, $PHCH_3$) 2.3 (s, 6H, $N(CH_3)_2$), 2.1 (t, 1H, CHCN). Anal. ($C_{19}H_{24}NCl$) C,H,N.

(±)-*trans*-1-(4-Chlorophenyl)-3-(*N*,*N*-dimethylamino)-1,2,3,4-tetrahydronaphthalene (22). The primary amine **90** (1.3 mg) was dimethylated as above to afford 1.4 g (97%) of a yellow-brown oil which was dissolved in ethereal HCl and the salt recrystallized from EtOH/Et_2O to afford 620 mg of colorless crystals (1.92 mmol, 38%): mp 256−258 °C; ^{1}H NMR ($CDCl_3$) δ 7.2−7.4 (m, 4H, ArH), 7.1−7.18 (m, 2H, ArH), 6.8−6.9 (m, 2H, ArH), 4.4 (t, 1H, PhCHPh), 3.0 (dd, 1H, PhCH), 2.8 (dd, 1H, PhCH), 2.6 (m, 1H, CHN), 2.2 (s, 6H, $N(CH_3)_2$), 2.0 (t, 1H, CHCN), 1.65 (m, 1H, CHCN). Anal. ($C_{18}H_{21}NCl_2$) C,H,N.

(±)-*trans*-1-(4-Methylphenyl)-3-(*N*,*N*-dimethylamino)-1,2,3,4-tetrahydronaphthalene (23). The primary amine **91** (180 mg, 0.67 mmol) was dimethylated as above to afford 180 mg (97%) of a light brown oil which was dissolved in ethereal HCl. The salt was recrystallized from ethanol/Et_2O to afford 39 mg (0.13 mmol, 19.4%) of colorless crystals: mp 252−253 °C; ^{1}H NMR ($CDCl_3$) δ 7.0−7.2 (m, 5H, ArH), 6.95 (d, 1H, ArH), 6.85 (dd, 1H, ArH), 4.4 (t, 1H, PhCHPh), 3.1 (dd, 1H, PhCH), 2.9 (dd, 1H, PhCH), 2.6 (m, 1H, CHN), 2.4 (s, 6H, $N(CH_3)_2$), 2.3 (s, 3H, $PhCH_3$) 2.1 (t, 1H, CHCN). Anal. ($C_{19}H_{24}NCl$) C,H,N.

(±)-*trans*-1-(4-Fluorophenyl)-3-(*N*,*N*-dimethylamino)-1,2,3,4-tetrahydronaphthalene (24). The primary amine **92** (345 mg, 1.28 mmol) was dimethylated as above to afford 150 mg (39%) of a pale yellow oil which was dissolved in ethereal HCl and the salt recrystallized from ethanol/Et_2O to afford 37 mg (0.12 mmol, 9.4%) of white crystals: mp: 210−212 °C; ^{1}H NMR ($CDCl_3$) δ 7.1−7.25 (m, 4H, ArH), 6.9 (m, 4H, ArH), 4.4 (t, 1H, PhCHPh), 3.15 (dd, 1H, PhCH), 3.0 (dd, 1H, PhCH), 2.9 (m, 1H, CHCN), 2.8 (m,1H, CHCN), 2.45 (s, 6H, $N(CH_3)_2$), 2.1 (m, 1H, CHN). Anal. ($C_{18}H_{21}NClF$) C,H,N.

(±)-*cis*-1-Phenyl-3-(trimethylammoniumyl)-1,2,3,4-tetrahydronaphthalene Iodide (25). Methyl iodide (1.5 mmol) in toluene was added to a solution of (±)-*cis*-1-phenyl-3-amino-1,2,3,4-tetrahydronaphthalene (75 mg, 0.299 mmol) in 20 mL of anhydrous ether, and the reaction mixture was allowed to stand at room temperature overnight. The methiodide salt precipitated and was filtered and dried to afford the crude product. Recrystallization from EtOH afforded 76 mg (65%) of pure product as yellow crystals: mp 260−262 °C; ^{1}H NMR ($CDCl_3$) δ 7.0−7.4 (m, 8H, ArH), 6.7 (d, 1H, ArH), 4.4 (dd, 1H, PhCHPh), 4.0 (m, 1H, CHN), 3.5 (t, 2H, PhCH), 3.2 (s, 9H, $N(CH_3)_3$), 2.7 (dd, 1H, CH_2), 2.1 (q, 1H, CH_2). Anal. ($C_{19}H_{21}NI$) C,H,N.

3-(Dimethylamino)fluoranthene (27). The primary amine 3-aminofluoranthene (**26**) (250 mg) was dissolved in 3 mL of 98% formic acid to which was added 2 mL of 37% of aqueous formaldehyde. The slurry was stirred at reflux 12 h. The volatiles were removed in vacuo, and the residue was partitioned between CH_2Cl_2 and saturated $NaHCO_3$. The organic phase was dried (Na_2SO_4) and evaporated in vacuo to afford a bright yellow powder. Recrystallization in MeOH/$CHCl_3$ yielded 65 mg of a yellow powder. Anal. ($C_{18}H_{15}N$) C,H,N.

Radioreceptor Binding Assays. Chemicals: [^{3}H]Mepyramine (23 Ci/mmol) was obtained from DuPont-NEN Corp. (Boston, MA). Synthesis and resolution of (±)-*trans*-H_2-PAT were as previously reported (Wyrick et al., 1993). (−)-*trans*-H_2-PAT subsequently was radiolabeled as previously reported (Wyrick et al., 1994) with tritiated methyl iodide to yield [*N*-^{3}H-methyl]-(1*R*,3*S*)-(−)-*trans*-1-phenyl-3-(dimethylamino)-1,2,3,4-tetrahydronaphthalene ([^{3}H]-(−)-*trans*-H_2-PAT) at 85 Ci/mmol. Other biochemical reagents were purchased or donated from Research Biochemicals Int. (RBI, Natick, MA).

Tissue preparation: Frozen guinea pig brain, minus cerebellum, was thawed and homogenized in 10 mL/g of tissue of cold buffer solution containing 10 mM TRIS and 0.32 M sucrose. The homogenate then was centrifuged at 1000*g* for 15 min at 4 °C. The supernatant was separated and recentrifuged at 31000*g* for an additional 15 min (4 °C). The P_2 pellet was resuspended in 10 mM TRIS buffer (pH 7.4, 25 °C) at 3 mL/g of original wet weight tissue and incubated for 15 min at 25 °C. This suspension was centrifuged at 31000*g* for 15 min (4 °C) with the resulting pellet resuspended with 10 mM TRIS buffer (pH 7.4, 25 °C) at a final volume of 1.5 mL/g of original wet weight tissue with gentle vortexing. The final tissue concentration was ca. 2.5−5 mg of protein/mL. Tissue was stored at −80 °C until use.

Competition binding assays: H_2-PAT isomers were incubated in triplicate borosilicate glass tubes (1 h, 30 °C) with 0.1 nM [^{3}H]-*trans*-H_2-PAT (10 mM TRIS, pH 7.4) or 2 nM [^{3}H]-mepyramine (50 mM Na^+K^+-phosphate, pH 7.4) protein from above preparation in a total assay volume of 1.0 mL (0.5 mL for DTG). Nonspecific binding was determined by 10.0 μM ketanserin for [^{3}H]-*trans*-H_2-PAT and 20.0 μM triprolidine for [^{3}H]mepyramine. After incubation, assay mixtures were filtered with a cell harvester through glass fiber (GF/B) sheets. Sheets were rinsed three times with 5−10 mL of cold buffer and counted for tritium by liquid scintillation spectrometry at 60% efficiency. Nonlinear regression analysis of inhibition data was used to determine IC_{50} values using Prism 2.0 (GraphPad, San Francisco, CA). IC_{50} values were converted to $K_{0.5}$ based upon the Cheng−Prussof equation where $K_{0.5}$ =

$IC_{50}/(1 + L^*/K_D)$.[30] Experiments were repeated at least three times to determine mean $K_{0.5} \pm$ SEM.

Acknowledgment. U.S. Public Health Service Grant NS35216 and the Pharmacy Foundation of North Carolina supported this investigation. The authors are grateful to Professor Richard B. Mailman for his interest in this work and helpful discussions. The authors thank Tripos Inc. for the generous provision of Sybyl 6.22 used for various phases of this work.

References

(1) Booth, R. G.; Wyrick, S. D.; Baldessarini, R. J.; Kula, N. S.; Myers, A. M.; Mailman, R. B. New *σ*-like Receptor Recognized by Novel Phenylaminotetralins: Ligand Binding and Functional Studies, *Mol. Pharmacol.* **1993**,*44*, 1232−1239.

(2) Wyrick, S. D.; Booth, R. G.; Myers, A. M.; Owens, C. E.; Kula, N. S.; Baldessarini, R. J.; McPhail, A. T.; Mailman, R. B. Synthesis and Pharmacological Evaluation of 1-phenyl-3-amino-1,2,3,4-tetrahydronaphthalenes as Ligands for a Novel Receptor with Neuromodulatory Sigma-like Activity. *J. Med. Chem.* **1993**, *36*, 2542−2551.

(3) Wyrick, S. D.; Myers, A. M.; Booth, R. G.; Kula, N. S.; Baldessarini, R. J. Synthesis of [*N*-C^3H_3]-*trans*-(1*R*,3*S*)-(−)-1-phenyl-3-*N*,*N*-(dimethylamino)-1,2,3,4-Tetrahydronaphthalene (H_2-PAT). *J. Labelled Compds. Radiopharm.* **1994**, *34*, 131−134.

(4) Owens, C. E.; Mailman, R. B.; Wyrick, S. D.; Booth, R. G. Putative σ_3 Sites in Mammalian Brain have Histamine H_1 Properties. *Soc. Neurosci. Abstr.* **1996**, *22*, 2006.

(5) Choksi, N. Y.; Wyrick, S. D.; Booth, R. G. Phenylaminotetralins Modulate Dopamine Synthesis in Rat Nucleus Accumbens In Vivo by a Presynaptic H_1 Type Receptor. *Soc. Neurosci. Abs.***1997**, *23*, 2036.

(6) Bucholtz, E. C.; Wyrick, S. D.; Brown, R. L.; Booth, R. G. Design of Phenylaminotetralins Selective for Proposed Histamine H_1 Receptor Subtypes in Mammalian Forebrain. *Soc. Neurosci. Abstr.* **1997**, *23*, 2036.

(7) Owens, C. E.; Myers, A. M.; Lawler, C. P.; Mailman, R. B.; Baldessarini, R. J.; Wyrick, S. D.; Booth, R. G. Characterization and Distribution of Brain σ_3 Receptors Labeled by [^{3}H]-(−)-*trans*-H_2-PAT. *Soc. Neurosci. Abstr.* **1994**, *20*, 748.

(8) Keduda, R.; Prasad, P. D.; Fei, Y.; Leibach, F. H.; Ganapathy, V. Cloning and Functional Expression of the Human Type 1 Sigma Receptor (hSigmaR1). *Biochem. Biophys. Res. Commun.* **1996**, *229*, 553−558.

(9) Hanner, M.; Moebius, F. F.; Flandorfer, A.; Knaus, H.; Striessing, J.; Kempner, E.; Glossmann, H. Purification, Molecular Cloning, and Expression of the Mammalian Sigma1-Binding Site. *Proc. Natl. Acad. Sci. U.S.A.* **1996**, *93*, 8072−8077.

(10) Saxena, A. K.; Saxena, M. Developments in Antihistamines (H_1)-. In *Progress in Drug Research*; Jucker, E., Ed.; Birhauser Verlag: Basel, 1992; Vol. 39 pp 35−125.

(11) Warringa, C. G.; Rekker, R. F.; Nauta, W. Th. 1,1-Diaryl-3-aminopropenes and Some Related Compounds II. Structure−Activity Relationships. *Eur. J. Med. Chem.* **1975**, *10*, 349−352.

(12) Ison, R. R.; Franks, F. M.; Soh, K. S. The Binding of Conformationally Restricted Antihistamines to Histamine Receptors. *J. Pharm. Pharmacol.* **1973**, *25*, 887−894.

(13) Miyano, S.; Abe, A.; Kase, Y.; Yuizono, T.; Tachibana, K.; Miyata, T.; Kito, G. Synthesis and Pharmacological Evaluation of Some Pyridylmethyl Substituted Ethylenediamines. *J. Med. Chem.* **1970**, *13*, 704−708

(14) Casy, A. F.; Ganellin, C. R.; Mercer, A. D.; Upton, C. Analogues of Triprolidine: Structural Influences upon Antihistamine Activity. *J. Pharm. Pharmacol.* **1992**, *44*, 791−795.

(15) Wyrick, S. D.; Booth, R. G.; Myers, A. M.; Owens, C. E.; Bucholtz, E. C.; Hooper, P. C.; Kula, N. S.; Baldessarini, R. G.; Mailman, R. B. 1-Phenyl-3-amino-1,2,3,4-tetrahydronaphthalenes and Related Derivatives as Ligands for the Neuromodulatory σ_3 receptor: Further Structure−Activity Relationships. *J. Med. Chem.* **1995**, *38*, 3857−3864.

(16) Myers, A. M.; Charifson, P. S.; Owens, C. E.; Kula, N. S.; McPhail, A. T.; Baldessarini, R. J.; Booth, R. G.; Wyrick, S. D. Conformational Analysis, Pharmacophore Identification and Comparative Molecular Field Analysis of Ligands for the Neuromodulatory σ_3 Receptor. *J. Med. Chem.* **1994**, *37*, 4109−4117.

(17) Martin, Y. C.; Bures, M. G.; Dahaner, E. A.; Delasser, J.; Lico, I.; Pavlik, P. A. A Fast Approach to Pharmacophore Mapping and its Application to Dopaminergic and Benzopdiazepine Agonists. *J. Comput.-Aid. Mol. Des.* **1993**, *7*, 83−102.

(18) Bucholtz, E. C.; Wyrick, S. D.; Owens, C. E.; McPhail, A. T.; Booth, R. G. 1-Phenyl-3-(dimethylamino)-1,2,3,4-tetrahydronaphthalene (H_2-PAT): Effect of Stereochemistry on Binding and Function at Brain Histamine Receptors. *Med. Chem. Res.* **1998**, *8*, 322−332.

(19) Laus, G.; Tourwe, D.; Van Binst, G. Benzo and indoquinolizidine derivatives XIX. Synthesis and Pharmacological Activity of Quinolizidine Derivatives. Analogues of Butaclamol. *Heterocycles* **1984,** *22*, 311−331.

(20) Eschweiler, W. Ersatz von an Stickstoff Gebundenun Wasserstoffatomen Durch die Methylgruppe mit Hilfe von Formaldhyd. *Ber.* **1905**, *38*, 880−882.

(21) The Sybyl program (version 6.22) is available from Tripos Associates, 1699 Hanley Rd, St. Louis, MO 63144.

(22) Cramer, R. D., III; Patterson, D. E.; Bunce, J. D. Comparative Molecular Field Analysis (CoMFA). 1. Effect of Shape on Binding of Steroids to Carrier Proteins. *J. Am. Chem. Soc.* **1988**, *110*, 5959−5967.

(23) Cho, S. J.; Tropsha, A. Cross-Validated R^2-Guided Region Selection for Comparative Molecular Field Analysis: A Simple Method to Achieve Consistent Results. *J. Med. Chem.* **1995**, *38*, 1060−1066.

(24) Leurs, R.; Smit, M. J.; Timmerman, H. Histaminergic Agonists and Antagonists: Recent Developments. In *Advances in Drug Research*; Testa, B., Ed.; Academic Press: London, 1991; Vol. 20, pp 217−30.

(25) Zhang, M. Q.; Leurs, R.; Timmerman, H. Histamine H_1 Receptor Antagonists. In *Burger's Medicinal Chemistry and Drug Discovery*, 5th ed.; Wolff, M., Ed.; John Wiley & Sons Inc.: New York, 1997.

(26) Nauta, W. T.; Rekker, R. F. Structure−Activity Relationships of H_1-Receptor Antagonists. In *Handbook of Experimental Pharmacology*; Rocha e Silva, M., Ed.; Springer-Verlag: New York, 1978.

(27) Protiva, M. Recent Progress in the Pharmaco-Chemical Research on Antihistamine Drugs and Psychotropic Agents- Derivatives of Tricyclic Systems Having a Seven or Eight-Membered Ring. *Farmaco Ed. Sci.* **1966**, *21*, 76−104.

(28) Ortiz, A. R.; Pastor, M.; Palomer, A.; Cruciani, G.; Gago, F.; Wade, R. C. Reliability of Comparative Molecular Field Analysis Models: Effects of Data Scaling and Variable Selection Using a Set of Human Synovial Fluid Phospholipase A2 Inhibitors. *J. Med. Chem.* **1997**, *40*, 1136−1148.

(29) Southwick, P. L.; Sapper, D. I. 4-Styrylthialzoles. Synthesis and Relationships Among Ultraviolet Absorption Spectra. *J. Org. Chem.* **1954,** *19*, 1926−1937.

(30) Cheng, Y. C.; Prusoff, W. H. Relationship between the inhibition constant (K1) and the concentration of inhibitor which causes 50% inhibition (I50) of an enzymatic reaction. *Biochem. Pharmacol.* **1973**, *22*, 3099−3108.

JM980428X